Robotica (2017) volume 35, pp. 537–568. © Cambridge University Press 2015
doi:10.1017/S0263574715000703

Dynamic modeling and characteristics analysis of lateral-pendulum unicycle robot

Yohanes Daud†, Abdullah Al Mamun‡ and Jian-Xin Xu§

†*Graduate Student in Department of Electrical and Computer Engineering, National University of Singapore, 4 Engineering Drive 3, 117576, Singapore. E-mail: yohanesdaud86@gmail.com*
‡*Associate Professor in Department of Electrical and Computer Engineering, National University of Singapore, 4 Engineering Drive 3, 117576 Singapore. E-mail: eleaam@nus.edu.sg*
§*Department of Electrical and Computer Engineering, National University of Singapore, 4 Engineering Drive 3, 117576 Singapore. E-mail: elexujx@nus.edu.sg*

(Accepted July 23, 2015. First published online: September 2, 2015)

SUMMARY

Lateral-pendulum unicycle robot is a type of single-wheeled mobile robot which utilizes an inverted pendulum mounted laterally for its stabilization and control. Even though this concept was first mentioned in the 1980s, it has not been sufficiently explored especially from the theoretical point of view. Therefore, this robot represents a niche which is still open for more thorough research. This paper presents four contributions to the research of this particular robot. First, the complete model of the robot dynamics is derived and this model can facilitate more accurate study of the robot's static and dynamic behaviors. Secondly, two important constants namely (1) *lateral-statics boundary* and (2) *lateral-statics constant*, which are useful for the lateral stabilization, are derived and analyzed. Thirdly, *turning constant*, required for the control of the turning motion, is derived and used to study the achievable path curvature in maneuvering control. Lastly, dynamics couplings during steady linear motion and steady circular motion are studied and the necessity of integral action in the lateral controller for circular motion is shown and explained. Throughout this paper, numerical simulation is used intensively and two case studies are presented to illustrate the concepts.

1. Introduction

Unicycle robot is a particular type of single-wheeled mobile robot which has its chassis located on top of its wheel and supported by the wheel shaft. This is in contrast to monocycle robot, which has its chassis contained inside its wheel.[8] The unicycle robot has been investigated since the 1980s and the research of this robot is motivated by several factors including (1) the study of nonlinear and unstable dynamics,[1] (2) the emulation of human intelligence[12] and (3) the search for better means of transportation. It is important to note that, even though the single-wheeled robots, which include both the unicycle robot and the monocycle robot, are statically unstable, they have a few potential advantages over multi-wheeled robots including good dynamic stability at high speed and excellent maneuverability.

Various mechanisms for the posture balancing and maneuvering of unicycle robot have been proposed in the literature. In 1987, Arnoldus Schoonwinkel constructed a computer-controlled unicycle with a rotating turntable mounted on top of its platform as part of his doctorate research in Stanford University.[1] A few years after Schoonwinkel's thesis was published, similar unicycles were also constructed by David W. Vos and Andreas H. von Flotow in Massachusetts Institute of Technology,[2] and by Zaiquan Sheng and Kazuo Yamafuji in the University of Electro-Communication.[12] Sheng and Yamafuji opted to use a three-blade propeller in replacement of a uniform turntable and they found that when the mass distribution of the propeller was not uniform,

* Corresponding author. E-mail: yohanesdaud86@gmail.com

https://doi.org/10.1017/S0263574715000703 Published online by Cambridge University Press

the stability of the unicycle improved. In 2006, S. Majima, T. Kasai and T. Kadohara from the University of Tsukuba developed a unicycle robot with a reaction wheel for its stabilization and control.[9] A modified version of this unicycle robot was constructed by Hongzhe Jin, Jongmyung Hwang and Jangmyung Lee in Pusan National University who used a two-blade propeller instead of a uniform reaction wheel.[3]

The idea of using a lateral pendulum for the stabilization and control of the unicycle robot was first conceived by Schoonwinkel in his doctorate thesis. He argued that, in order to properly emulate a human riding a unicycle, a unicycle robot should ideally be equipped with a lateral pendulum and a turntable, which respectively mimic the movements of human hip and arms. However, he did not incorporate the lateral-pendulum mechanism into his unicycle design for simplicity reason.

The implementation of a lateral pendulum for controlling a single-wheeled mobile robot was first reported by Ryo Nakajima, Takashi Tsubouchi, Shin'ichi Yuta and Eiji Koyanagi from the University of Tsukuba.[7] In their paper, the development of Yamabico ICHIRO, a mobile robot having a single wheel with the shape of a rugby ball, is presented in great detail. The robot's head can lean sidewards for turning and, hence, it is a lateral-pendulum unicycle robot in principle. The robot dynamics was modeled by first separating its motion into longitudinal motion and lateral motion. Motion-control experiment with this robot was claimed to be successful. The rugby-ball shaped wheel has improved the robot's stability in the lateral direction greatly, so it does not seem fair to compare Yamabico ICHIRO with the other unicycle robots with the classic pneumatic wheels, in which the lateral instability is a very challenging problem.

The development of the first true lateral-pendulum unicycle robot was first reported by Yasutaka Fujimoto and Shuhei Uchida from Yokohama National University in 2007.[11] Similar to the work of Nakajima *et al.*, the dynamic model of their robot was derived by first separating its motion in two directions: longitudinal motion and lateral motion. The dynamic model for turning motion was derived separately from the concept of centripetal motion. In addition to the modeling, they also designed simple controllers and observers, and conducted some simulation study. A figure of their robot prototype is shown in the paper and experimental work is put as the future work. However, until recently, we have not been able to find any more publication related to their work. This leads us to speculate that the experimental work of that robot is much more challenging than the simulation results have suggested.

Aside from the work of the two groups of Japanese researchers above, to the best of our knowledge, there are no other research groups working on the lateral-pendulum unicycle robot. Our literature review returns the following findings.

(1) *Inavailability of complete dynamic model:* All dynamic models of the lateral-pendulum unicycle robot currently available in the literature are developed by initially separating the robot motion into two directions: longitudinal motion and lateral motion. As a consequence, the resulting models do not have information about the couplings among all of the robot dynamics. Therefore, simulation studies with these models are oversimplified, especially if they involve turning motion.
(2) *Absence of analyses for successful posture balancing and maneuvering:* Unicycle is an inherently unstable system with highly nonlinear dynamics. Aside from being unstable and nonlinear, this robot is also underactuated and non-minimum phase. Therefore, before even designing and implementing a control scheme for a certain control task, it is natural to ask whether the given task is possible in the first place and if it is possible, how difficult it is. These analyses are currently not available in the literature.
(3) *No reported successful implementation:* As of the year 2014, there is currently no reported successful realization of the true lateral-pendulum unicycle robot, i.e. the lateral-pendulum unicycle robot with the classic pneumatic wheel.

In view of these findings, through this paper, we present some results of our work on the lateral-pendulum unicycle robot which partially fill the gap in the research of this robot. We have been developing a prototype of this robot since 2011. Even though autonomy capability has not been achieved yet, we have constructed the mechanical structure of the robot and equipped it with the basic electronic system. Our robot is named *ALP Cycle*, which stands for *Automatic Lateral-Pendulum Unicycle*. Figure 1 shows the conceptual design of the ALP Cycle with the description of its parts and degrees of freedom. As part of the development process, the mathematical model of the robot,

https://doi.org/10.1017/S0263574715000703 Published online by Cambridge University Press

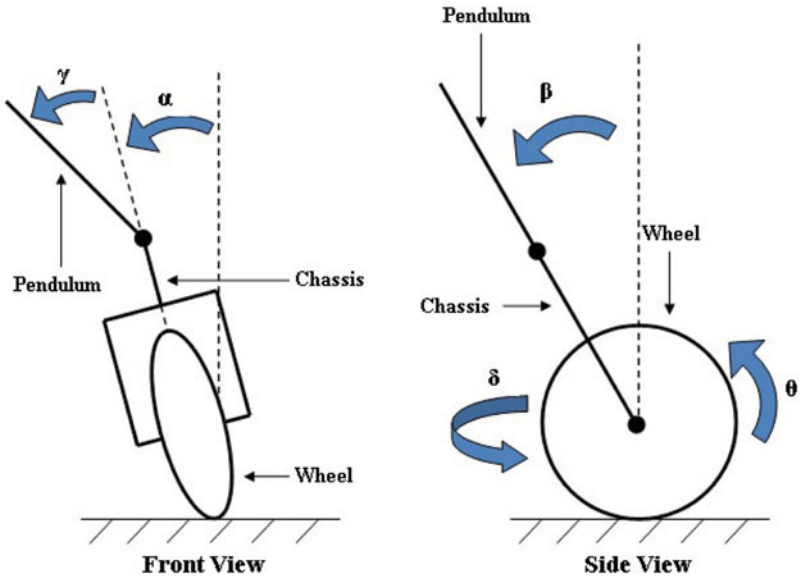


Fig. 1. The conceptual design of the ALP Cycle.

a very important element for thorough simulation study and control design, has been developed and analyzed. The model development and analyses form the core of this paper.

This paper is organized as followed. In Section 2, the complete dynamic model of the lateral-pendulum unicycle robot is derived by Euler–Lagrange formulation. In Section 3, the resulting nonlinear model is simplified by pseudolinearization with respect to the robot's upright posture in order to get a reasonably simpler model for analyses. In Section 4, the robot characteristics are evaluated and several important constants needed for the designs of lateral controller and turning controller are derived. The usefulness of these constants is illustrated by two case studies. Lastly, Section 5 draws some concluding remarks.

2. Dynamic Modeling

In the modeling of any dynamical system by means of mathematical derivation and physical principles, three methods are available: Newton method, Euler–Lagrange method and Hamilton method. In this paper, Euler–Lagrange method is chosen because it provides a straightforward and simple way of model derivation for complex systems such as the ALP Cycle. The method does not involve redundant forces and torques, so it is less prone to errors in comparison with Newton method.

In what follows, the modeling assumptions, coordinate frames, generalized coordinates, generalized forces, system's parameters and kinematic constraints are first defined. Subsequently, the modeling process follows a standard procedure which involves the computations of position vectors, velocity vectors, kinetic energies, potential energies and Lagrangian.[6]

2.1. Modeling assumptions

The following six assumptions are used in the modeling process.

(1) The ALP Cycle consists of three links or bodies: wheel, chassis and pendulum. All electronics and mechanical parts other than the wheel, chassis and pendulum are assumed to be parts of these three bodies.
(2) The wheel, chassis and pendulum are perfectly rigid bodies.
(3) The ALP Cycle is perfectly symmetric with respect to its sagittal and coronal planes.
(4) The ground, on which the ALP Cycle moves on, is perfectly flat.
(5) The wheel is always in contact with the ground.
(6) There is no slip between the wheel and the ground.

https://doi.org/10.1017/S0263574715000703 Published online by Cambridge University Press

2.2. Coordinate frames, generalized coordinates & generalized forces

One inertial coordinate frame and six body coordinate frames are defined and assigned. These seven coordinate frames are described one by one below.

(1) *Inertial coordinate frame* denoted by $\Sigma_G(x_g, y_g, z_g)$: The origin of this frame, the x_g axis and the y_g axis are placed on the ground's surface. This frame is anchored to the ground and, therefore, it is always static.
(2) *Contact-point coordinate frame* denoted by $\Sigma_{CP}(x_{cp}, y_{cp}, z_{cp})$: The origin of this frame is placed at the contact point between the wheel and the ground. The x_{cp} and y_{cp} axes are always on the ground's surface. In addition, the x_{cp} axis defines the forward direction of the ALP Cycle.
(3) *Wheel coordinate frame 1* denoted by $\Sigma_{W1}(x_{w1}, y_{w1}, z_{w1})$: The origin of this frame is placed at the center of mass of the wheel. The x_{w1} and y_{w1} axes are always parallel to the ground's surface. Although, this frame is attached to the wheel, it does not rotate together with the wheel.
(4) *Wheel coordinate frame 2* denoted by $\Sigma_{W2}(x_{w2}, y_{w2}, z_{w2})$: The origin of this frame is placed at the center of mass of the wheel. The x_{w2} axis is always aligned with the x_{w1} axis. Although this frame is attached to the wheel, it does not rotate together with the wheel, but it leans sidewards together with the wheel.
(5) *Wheel coordinate frame 3* denoted by $\Sigma_{W3}(x_{w3}, y_{w3}, z_{w3})$: The origin of this frame is placed at the center of mass of the wheel. The y_{w3} axis is always aligned with the y_{w2} axis. This frame rotates together with the wheel.
(6) *Chassis coordinate frame* denoted by $\Sigma_C(x_c, y_c, z_c)$: The origin of this frame is placed at the center of mass of the chassis. The y_c axis is always parallel to the y_{w2} axis.
(7) *Pendulum coordinate frame* denoted by $\Sigma_P(x_p, y_p, z_p)$: The origin of this frame is placed at the center of mass of the pendulum. The x_p axis is always parallel to the x_c axis.

The placements of the seven coordinate frames are illustrated in Fig. 2 where the *inertial frame* (Σ_G), *contact-point frame* (Σ_{CP}), *wheel frame 1* (Σ_{W1}), *wheel frame 2* (Σ_{W2}), *wheel frame 3* (Σ_{W3}), *chassis frame* (Σ_C) and *pendulum frame* (Σ_P) are in black, olive green, red, blue, orange, green and purple respectively.

Based on the assigned coordinate frames, the following seven generalized coordinates are identified.

- x: the position of the contact point between the wheel and the ground from the origin of Σ_g along the x_g axis.
- y: the position of the contact point between the wheel and the ground from the origin of Σ_g along the y_g axis.
- θ: the angle formed by the z_{w3} axis and the z_{w2} axis. θ represents the angular position of the wheel with respect to the chassis' upright posture. It is called *wheel angle*.
- α: the angle formed by the z_{w2} axis and the z_{w1} axis. α represents the angular position of the wheel and chassis in the lateral direction with respect to the upright posture of the wheel and chassis. It is called *lateral lean angle* or simply *lean angle* or *roll angle*.
- β: the angle formed by the z_c axis and the z_{w2} axis. β represents the angular position of the chassis in the longitudinal direction with respect to the chassis' upright posture. It is called *longitudinal lean angle* or *pitch angle*.
- γ: the angle formed by the z_p axis and the z_c axis. γ represents the angular position of the pendulum with respect to the chassis. It is called *pendulum angle*.
- δ: the angle formed by the x_{cp} axis and the x_g axis. δ represents the angular position of the wheel with respect to the x_g axis. It is called *turning angle* or *yaw angle*.

There are two generalized forces in the system corresponding to the usage of two actuators. They are as followed.

- τ_w: the torque input by the wheel motor to actuate the wheel.
- τ_p: the torque input by the pendulum motor to actuate the pendulum.

2.3. Parameters

The ALP Cycle's physical parameters, which include the links' lengths, links' masses and links' principal moments of inertia, and the environmental parameter, which is the gravitational acceleration,

https://doi.org/10.1017/S0263574715000703 Published online by Cambridge University Press

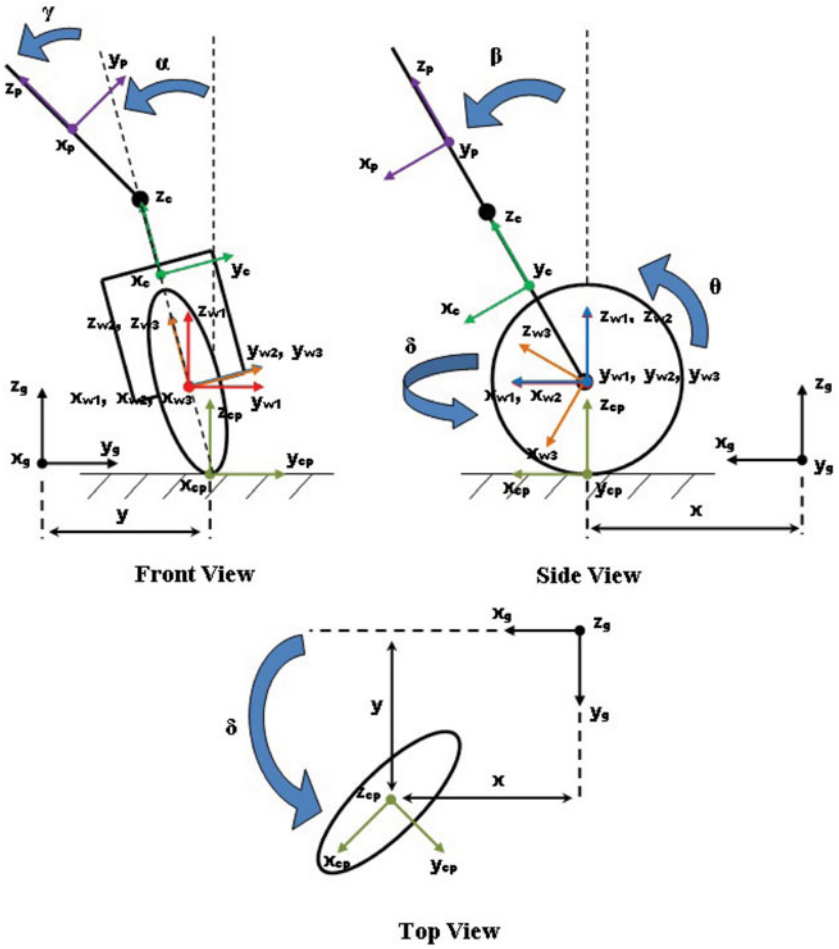


Fig. 2. The definitions and assignments of the inertial frame and body frames.

are described in Table I and illustrated in Fig. 3. The values of these parameters are computed from the 3-D CAD model of the robot developed in SolidWorks.

2.4. Kinematic constraints

Since it is assumed that the wheel rotates on the ground without slipping, it is a well-known fact that the velocity of the contact point between the wheel and the ground with respect to the inertial coordinate frame, V_{cnt}, is zero. This can be expressed by Eq. (1).

$$V_{cnt} = \begin{bmatrix} \dot{x} - r_w\dot{\theta}\cos(\delta) \\ \dot{y} - r_w\dot{\theta}\sin(\delta) \\ \dot{z} \end{bmatrix} = \begin{bmatrix} 0 \\ 0 \\ 0 \end{bmatrix}. \tag{1}$$

Therefore, the robot motion satisfies the following kinematic constraints.

$$\dot{x} = r_w\dot{\theta}\cos(\delta) \tag{2}$$

$$\dot{y} = r_w\dot{\theta}\sin(\delta) \tag{3}$$

$$\dot{z} = 0. \tag{4}$$

Equations (2) and (3) are non-integrable, so they are said to be nonholonomic.

https://doi.org/10.1017/S0263574715000703 Published online by Cambridge University Press

Table I. Description of the ALP Cycle's physical and environmental parameters.

Symbol	Description	Value & Unit
m_w	Wheel mass	1.42 kg
m_c	Chassis mass	6.34 kg
m_p	Pendulum mass	0.85 kg
I_{w1}	Wheel x-dir. moment of inertia	0.01 kg · m^2
I_{w2}	Wheel y-dir. moment of inertia	0.02 kg · m^2
I_{w3}	Wheel z-dir. moment of inertia	0.01 kg · m^2
I_{c1}	Chassis x-dir. moment of inertia	0.17 kg · m^2
I_{c2}	Chassis y-dir. moment of inertia	0.11 kg · m^2
I_{c3}	Chassis z-dir. moment of inertia	0.08 kg · m^2
I_{p1}	Pendulum x-dir. moment of inertia	0.03 kg · m^2
I_{p2}	Pendulum y-dir. moment of inertia	0.03 kg · m^2
I_{p3}	Pendulum z-dir. moment of inertia	0.0003 kg · m^2
r_w	Wheel radius	0.15 m
l_c	Distance between wheel center of mass and chassis center of mass	0.15 m
l_{cp}	Distance between chassis center of mass and pendulum pivot	0.13 m
l_p	Distance between pendulum pivot and center of mass	0.41 m
g	Gravitational acceleration	9.81 m/s^2

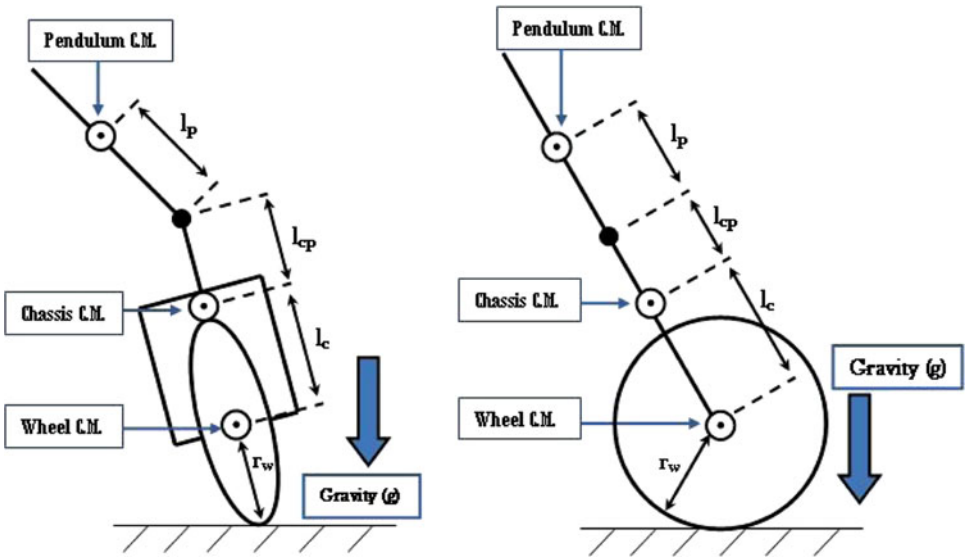


Fig. 3. Illustration of the ALP cycle's physical parameters and environmental parameter (C.M.: Center of Mass).

2.5. Lagrange equation

By Euler–Lagrange formulation, the mathematical model of any dynamical system can be derived by solving the following Lagrange equation:

$$\frac{d}{dt}\left(\frac{\partial L}{\partial \dot{q}_i}\right) - \frac{\partial L}{\partial q_i} = Q_i + \sum_{k=1}^{n} \lambda_k a_{ki} \tag{5}$$

$$i = 1 \ldots m,$$

where L is the *Lagrangian*, q_i is the *generalized coordinate*, Q_i is the *generalized force*, m is the number of generalized coordinates, n is the number of kinematic constraints, λ_k is *Lagrange multiplier* and a_{ki} is a variable which depends on the kinematic constraints.

https://doi.org/10.1017/S0263574715000703 Published online by Cambridge University Press

The Lagrangian of a system is the difference between the system's total kinetic energy T_{total} and total potential energy P_{total}.

$$L = T_{total} - P_{total}. \tag{6}$$

The kinetic and potential energies of the wheel, chassis and pendulum are functions of the position, linear velocity and angular velocity of the center of mass of the respective body. Therefore, in what follows, we shall proceed from the bottom up by computing these quantities first and, then, continuing with the computations of energies and Lagrangian before finally solving the Lagrange equation to get the final dynamic model.

2.5.1. Position vectors. The position vectors of the centers of mass of the wheel, chassis and pendulum with respect to the inertial frame are determined by using the homogeneous-transformation matrices among the coordinate systems.

In order to find the position of the wheel's center of mass, we need the transformation matrix ${}^{g}_{w2}T$, which maps the frame Σ_{w2} into the frame Σ_g. From Fig. 2, the transformation matrix ${}^{cp}_{w2}T$ defining the frame Σ_{w2} with respect to the frame Σ_{cp} and the transformation matrix ${}^{g}_{cp}T$ defining the frame Σ_{cp} with respect to the frame Σ_g are as followed.

$$\begin{aligned} {}^{cp}_{w2}T &= \begin{bmatrix} 1 & 0 & 0 & 0 \\ 0 & \cos(\alpha) & -\sin(\alpha) & 0 \\ 0 & \sin(\alpha) & \cos(\alpha) & 0 \\ 0 & 0 & 0 & 1 \end{bmatrix} \begin{bmatrix} 1 & 0 & 0 & 0 \\ 0 & 1 & 0 & 0 \\ 0 & 0 & 1 & r_w \\ 0 & 0 & 0 & 1 \end{bmatrix} \\ &= \begin{bmatrix} 1 & 0 & 0 & 0 \\ 0 & \cos(\alpha) & -\sin(\alpha) & -r_w \sin(\alpha) \\ 0 & \sin(\alpha) & \cos(\alpha) & r_w \cos(\alpha) \\ 0 & 0 & 0 & 1 \end{bmatrix} \end{aligned} \tag{7}$$

$${}^{g}_{cp}T = \begin{bmatrix} \cos(\delta) & -\sin(\delta) & 0 & x \\ \sin(\delta) & \cos(\delta) & 0 & y \\ 0 & 0 & 1 & 0 \\ 0 & 0 & 0 & 1 \end{bmatrix} \tag{8}$$

The transformation matrix ${}^{g}_{w2}T$ is the result of the multiplication of the transformation matrices ${}^{g}_{cp}T$ and ${}^{cp}_{w2}T$:

$$\begin{aligned} {}^{g}_{w2}T &= {}^{g}_{cp}T \times {}^{cp}_{w2}T \\ &= \begin{bmatrix} \cos(\delta) & {}^{g}_{w2}t_{12} & {}^{g}_{w2}t_{13} & {}^{g}_{w2}t_{14} \\ \sin(\delta) & {}^{g}_{w2}t_{22} & {}^{g}_{w2}t_{23} & {}^{g}_{w2}t_{24} \\ 0 & \sin(\alpha) & \cos(\alpha) & r_w \cos(\alpha) \\ 0 & 0 & 0 & 1 \end{bmatrix} \end{aligned} \tag{9}$$

where

- ${}^{g}_{w2}t_{12} = -\sin(\delta)\cos(\alpha)$
- ${}^{g}_{w2}t_{13} = \sin(\delta)\sin(\alpha)$
- ${}^{g}_{w2}t_{14} = x + r_w \sin(\delta)\sin(\alpha)$
- ${}^{g}_{w2}t_{22} = \cos(\delta)\cos(\alpha)$
- ${}^{g}_{w2}t_{23} = -\cos(\delta)\sin(\alpha)$
- ${}^{g}_{w2}t_{24} = y - r_w \cos(\delta)\sin(\alpha)$.

https://doi.org/10.1017/S0263574715000703 Published online by Cambridge University Press

In the frame Σ_{w2}, the position of the wheel's center of mass is ${}^{w2}P_w = [0 \quad 0 \quad 0 \quad 1]^T$. The position of the wheel's center of mass in the inertial frame, ${}^{g}P_w$, can be computed as followed.

$$\begin{aligned} {}^{g}P_w &= {}^{g}_{w2}T \times {}^{w2}P_w \\ &= \begin{bmatrix} x + r_w \sin(\alpha)\sin(\delta) \\ y - r_w \sin(\alpha)\cos(\delta) \\ r_w \cos(\alpha) \\ 1 \end{bmatrix}. \end{aligned} \tag{10}$$

For computing the position of the chassis' center of mass, the transformation matrix ${}^{g}_{c}T$, which maps the frame Σ_c into the frame Σ_g, is required. From Fig. 2, the transformation matrix ${}^{w2}_{c}T$, defining the frame Σ_c with respect to the frame Σ_{w2}, is as followed.

$$\begin{aligned} {}^{w2}_{c}T &= \begin{bmatrix} \cos(\beta) & 0 & \sin(\beta) & 0 \\ 0 & 1 & 0 & 0 \\ -\sin(\beta) & 0 & \cos(\beta) & 0 \\ 0 & 0 & 0 & 1 \end{bmatrix} \begin{bmatrix} 1 & 0 & 0 & 0 \\ 0 & 1 & 0 & 0 \\ 0 & 0 & 1 & l_c \\ 0 & 0 & 0 & 1 \end{bmatrix} \\ &= \begin{bmatrix} \cos(\beta) & 0 & \sin(\beta) & l_c \sin(\beta) \\ 0 & 1 & 0 & 0 \\ -\sin(\beta) & 0 & \cos(\beta) & l_c \cos(\beta) \\ 0 & 0 & 0 & 1 \end{bmatrix}. \end{aligned} \tag{11}$$

The transformation matrix ${}^{g}_{c}T$ can then be computed by multiplying the transformation matrices ${}^{g}_{w2}T$ and ${}^{w2}_{c}T$:

$$\begin{aligned} {}^{g}_{c}T &= {}^{g}_{w2}T \times {}^{w2}_{c}T \\ &= \begin{bmatrix} {}^{g}_{c}t_{11} & {}^{g}_{c}t_{12} & {}^{g}_{c}t_{13} & {}^{g}_{c}t_{14} \\ {}^{g}_{c}t_{21} & {}^{g}_{c}t_{22} & {}^{g}_{c}t_{23} & {}^{g}_{c}t_{24} \\ -\cos(\alpha)\sin(\beta) & \sin(\alpha) & \cos(\alpha)\cos(\beta) & {}^{g}_{c}t_{34} \\ 0 & 0 & 0 & 1 \end{bmatrix}, \end{aligned} \tag{12}$$

where

- ${}^{g}_{c}t_{11} = \cos(\beta)\cos(\delta) - \sin(\alpha)\sin(\beta)\sin(\delta)$
- ${}^{g}_{c}t_{12} = -\sin(\delta)\cos(\alpha)$
- ${}^{g}_{c}t_{13} = \sin(\beta)\cos(\delta) + \sin(\alpha)\cos(\beta)\sin(\delta)$
- ${}^{g}_{c}t_{14} = x + r_w \sin(\delta)\sin(\alpha) + l_c \sin(\beta)\cos(\delta) + l_c \sin(\alpha)\cos(\beta)\sin(\delta)$
- ${}^{g}_{c}t_{21} = \cos(\beta)\sin(\delta) + \sin(\alpha)\sin(\beta)\cos(\delta)$
- ${}^{g}_{c}t_{22} = \cos(\delta)\cos(\alpha)$
- ${}^{g}_{c}t_{23} = \sin(\beta)\sin(\delta) - \sin(\alpha)\cos(\beta)\cos(\delta)$
- ${}^{g}_{c}t_{24} = y - r_w \cos(\delta)\sin(\alpha) + l_c \sin(\beta)\sin(\delta) - l_c \sin(\alpha)\cos(\beta)\cos(\delta)$
- ${}^{g}_{c}t_{34} = r_w \cos(\alpha) + l_c \cos(\alpha)\cos(\beta)$.

In the frame Σ_c, the position of the chassis' center of mass is ${}^{c}P_c = [0 \quad 0 \quad 0 \quad 1]^T$. In the inertial frame, the position of the chassis' center of mass, ${}^{g}P_c$, is computed as:

$$\begin{aligned} {}^{g}P_c &= {}^{g}_{c}T \times {}^{c}P_c \\ &= \begin{bmatrix} {}^{g}p_{c1} \\ {}^{g}p_{c2} \\ {}^{g}p_{c3} \\ 1 \end{bmatrix}, \end{aligned} \tag{13}$$

https://doi.org/10.1017/S0263574715000703 Published online by Cambridge University Press

where

- ${}^{g}p_{c1} = x + r_w \sin(\alpha)\sin(\delta) + l_c \cos(\beta)\sin(\alpha)\sin(\delta) + l_c \sin(\beta)\cos(\delta)$
- ${}^{g}p_{c2} = y - r_w \sin(\alpha)\cos(\delta) - l_c \cos(\beta)\sin(\alpha)\cos(\delta) + l_c \sin(\beta)\sin(\delta)$
- ${}^{g}p_{c3} = r_w \cos(\alpha) + l_c \cos(\beta)\cos(\alpha)$.

We also need the transformation matrix ${}^{g}_{p}T$, mapping the frame Σ_p into the frame Σ_g, in order to find the position of the pendulum's center of mass. By referring to Fig. 2, the transformation matrix ${}^{c}_{p}T$, defining the frame Σ_p with respect to the frame Σ_c, can be calculated as followed.

$$
\begin{aligned}
{}^{c}_{p}T &= \begin{bmatrix} 1 & 0 & 0 & 0 \\ 0 & 1 & 0 & 0 \\ 0 & 0 & 1 & l_{cp} \\ 0 & 0 & 0 & 1 \end{bmatrix} \begin{bmatrix} 1 & 0 & 0 & 0 \\ 0 & \cos(\gamma) & -\sin(\gamma) & 0 \\ 0 & \sin(\gamma) & \cos(\gamma) & 0 \\ 0 & 0 & 0 & 1 \end{bmatrix} \\
&\quad \begin{bmatrix} 1 & 0 & 0 & 0 \\ 0 & 1 & 0 & 0 \\ 0 & 0 & 1 & l_p \\ 0 & 0 & 0 & 1 \end{bmatrix} \\
&= \begin{bmatrix} 1 & 0 & 0 & 0 \\ 0 & \cos(\gamma) & -\sin(\gamma) & -l_p \sin(\gamma) \\ 0 & \sin(\gamma) & \cos(\gamma) & l_{cp} + l_p \cos(\gamma) \\ 0 & 0 & 0 & 1 \end{bmatrix}.
\end{aligned} \tag{14}
$$

The transformation matrix ${}^{g}_{p}T$ is the product of the transformation matrices ${}^{g}_{c}T$ and ${}^{c}_{p}T$, and is given as:

$$
\begin{aligned}
{}^{g}_{p}T &= {}^{g}_{c}T \times {}^{c}_{p}T \\
&= \begin{bmatrix} \cos(\delta) & {}^{g}_{p}t_{12} & {}^{g}_{p}t_{13} & {}^{g}_{p}t_{14} \\ \sin(\delta) & {}^{g}_{p}t_{22} & {}^{g}_{p}t_{23} & {}^{g}_{p}t_{24} \\ 0 & {}^{g}_{p}t_{32} & {}^{g}_{p}t_{33} & {}^{g}_{p}t_{34} \\ 0 & 0 & 0 & 1 \end{bmatrix}.
\end{aligned} \tag{15}
$$

where

- ${}^{g}_{p}t_{12} = -\sin(\delta)\cos(\alpha)\cos(\gamma) + \cos(\delta)\sin(\beta)\sin(\gamma) + \sin(\delta)\sin(\alpha)\cos(\beta)\sin(\gamma)$,
- ${}^{g}_{p}t_{13} = \sin(\delta)\cos(\alpha)\sin(\gamma) + \cos(\delta)\sin(\beta)\cos(\gamma) + \sin(\delta)\sin(\alpha)\cos(\beta)\cos(\gamma)$,
- ${}^{g}_{p}t_{14} = l_p \sin(\delta)\cos(\alpha)\sin(\gamma) + (l_{cp} + l_p \cos(\gamma))(\cos(\delta)\sin(\beta) + \sin(\delta)\sin(\alpha)\cos(\beta)) + l_c \sin(\beta)\cos(\delta) + l_c \cos(\beta)\sin(\delta)\sin(\alpha) + x + r_w \sin(\delta)\sin(\alpha)$,
- ${}^{g}_{p}t_{22} = \cos(\delta)\cos(\alpha)\cos(\gamma) + \sin(\delta)\sin(\beta)\sin(\gamma) - \cos(\delta)\sin(\alpha)\cos(\beta)\sin(\gamma)$,
- ${}^{g}_{p}t_{23} = -\cos(\delta)\cos(\alpha)\sin(\gamma) + \sin(\delta)\sin(\beta)\cos(\gamma) - \cos(\delta)\sin(\alpha)\cos(\beta)\cos(\gamma)$,
- ${}^{g}_{p}t_{24} = -l_p \cos(\delta)\cos(\alpha)\sin(\gamma) + (l_{cp} + l_p \cos(\gamma))(\sin(\delta)\sin(\beta) - \cos(\delta)\sin(\alpha)\cos(\beta)) + l_c \sin(\beta) sin(\delta) - l_c \cos(\beta)\cos(\delta)\sin(\alpha) + y - r_w \cos(\delta)\sin(\alpha)$,
- ${}^{g}_{p}t_{32} = \sin(\alpha)\cos(\gamma) + \cos(\alpha)\cos(\beta)\sin(\gamma)$,
- ${}^{g}_{p}t_{33} = -\sin(\alpha)\sin(\gamma) + \cos(\alpha)\cos(\beta)\cos(\gamma)$,
- ${}^{g}_{p}t_{34} = -l_p \sin(\alpha)\sin(\gamma) + (l_{cp} + l_p \cos(\gamma))\cos(\alpha)\cos(\beta) + l_c \cos(\beta)\cos(\alpha) + r_w \cos(\alpha)$.

In the frame Σ_p, the position of the pendulum's center of mass is ${}^{p}P_p = \begin{bmatrix} 0 & 0 & 0 & 1 \end{bmatrix}^T$. The position of the pendulum's center of mass in the inertial frame, ${}^{g}P_p$, is computed as:

https://doi.org/10.1017/S0263574715000703 Published online by Cambridge University Press

$$
\begin{aligned}
{}^{g}P_p &= {}^{g}_{p}T \times {}^{p}P_p \\
&= \begin{bmatrix} {}^{g}p_{p1} \\ {}^{g}p_{p2} \\ {}^{g}p_{p3} \\ 1 \end{bmatrix}.
\end{aligned} \tag{16}
$$

where

- ${}^{g}p_{p1} = x + r_w \sin(\alpha)\sin(\delta) + (l_c + l_{cp})\cos(\beta)\sin(\alpha)\sin(\delta) + (l_c + l_{cp})\sin(\beta)\cos(\delta) + l_p \cos(\gamma)\cos(\beta)\sin(\alpha)\sin(\delta) + l_p \cos(\gamma)\sin(\beta)\cos(\delta) + l_p \sin(\gamma)\cos(\alpha)\sin(\delta)$,
- ${}^{g}p_{p2} = y - r_w \sin(\alpha)\cos(\delta) - (l_c + l_{cp})\cos(\beta)\sin(\alpha)\cos(\delta) + (l_c + l_{cp})\sin(\beta)\sin(\delta) - l_p \cos(\gamma)\cos(\beta)\sin(\alpha)\cos(\delta) + l_p \cos(\gamma)\sin(\beta)\sin(\delta) - l_p \sin(\gamma)\cos(\alpha)\cos(\delta)$,
- ${}^{g}p_{p3} = r_w \cos(\alpha) + (l_c + l_{cp})\cos(\beta)\cos(\alpha) + l_p \cos(\gamma)\cos(\beta)\cos(\alpha) - l_p \sin(\gamma)\sin(\alpha)$.

In the subsequent discussion, it is more convenient to work with 3×1 position vectors instead of the 4×1 position vectors above. Therefore, in what follows, we define P_w, P_c and P_p to be 3×1 position vectors made up of the first three elements of ${}^{g}P_w$, ${}^{g}P_c$ and ${}^{g}P_p$ respectively.

2.5.2. Linear velocity vectors. The linear velocity vectors of the wheel, chassis and pendulum can be directly derived from the respective position vectors by differentiation with respect to time.

- Wheel's linear velocity vector:

$$V_w = \frac{dP_w}{dt}, \tag{17}$$

- Chassis' linear velocity vector:

$$V_c = \frac{dP_c}{dt}, \tag{18}$$

- Pendulum's linear velocity vector:

$$V_p = \frac{dP_p}{dt}. \tag{19}$$

The expressions for linear velocity vectors for the three bodies are very complex, but since their derivations are straightforward, presenting their complete expressions here serves no purpose.

2.5.3. Angular velocity vectors. The angular velocity vectors of the wheel, chassis and pendulum must be expressed with respect to the frames Σ_{w2}, Σ_c and Σ_p respectively, so that, in the computation of angular kinetic energies, the moments of inertia of the wheel, chassis and pendulum appear as diagonal matrices. Therefore, the computation is greatly simplified. It must be noted, however, that this way of computation requires an implicit assumption that the frames Σ_{w2}, Σ_c and Σ_p are aligned with the principal frames of the wheel, chassis and pendulum respectively. Fortunately, since the bodies of the ALP Cycle is symmetric, this is a valid assumption.

The wheel's velocity vector is made up of three velocity components, which are the wheel velocity $\dot{\omega}$, the lean angular velocity $\dot{\alpha}$ and the turning velocity $\dot{\delta}$. These velocity components are expressed in different coordinate frames, so they are first mapped into the frame Σ_{w2} and the wheel's velocity

https://doi.org/10.1017/S0263574715000703 Published online by Cambridge University Press

vector with respect to the frame Σ_{w2}, Ω_w, is given by:

$$\begin{aligned}\Omega_w &= \begin{bmatrix}0\\ \dot{\theta}\\ 0\end{bmatrix} + \begin{bmatrix}\dot{\alpha}\\ 0\\ 0\end{bmatrix} + {}^{w2}_{g}T \times \begin{bmatrix}0\\ 0\\ \dot{\delta}\end{bmatrix}\\ &= \begin{bmatrix}0\\ \dot{\theta}\\ 0\end{bmatrix} + \begin{bmatrix}\dot{\alpha}\\ 0\\ 0\end{bmatrix} + {}^{g}_{w2}T^{-1} \times \begin{bmatrix}0\\ 0\\ \dot{\delta}\end{bmatrix}\\ &= \begin{bmatrix}\dot{\alpha}\\ \dot{\theta} + \dot{\delta}\sin(\alpha)\\ \dot{\delta}\cos(\alpha)\end{bmatrix}.\end{aligned} \tag{20}$$

The chassis' velocity vector consists of three velocity components, which are the longitudinal lean angular velocity $\dot{\beta}$, the lean angular velocity $\dot{\alpha}$ and the turning velocity $\dot{\delta}$. The three velocity components are expressed in different coordinate frames, so they are first mapped into the frame Σ_c and the chassis' velocity vector with respect to the frame Σ_c, Ω_c, is given by:

$$\begin{aligned}\Omega_c &= \begin{bmatrix}0\\ \dot{\beta}\\ 0\end{bmatrix} + {}^{c}_{w2}T \times \begin{bmatrix}\dot{\alpha}\\ 0\\ 0\end{bmatrix} + {}^{c}_{g}T \times \begin{bmatrix}0\\ 0\\ \dot{\delta}\end{bmatrix}\\ &= \begin{bmatrix}0\\ \dot{\beta}\\ 0\end{bmatrix} + {}^{w2}_{c}T^{-1} \times \begin{bmatrix}\dot{\alpha}\\ 0\\ 0\end{bmatrix} + {}^{g}_{c}T^{-1} \times \begin{bmatrix}0\\ 0\\ \dot{\delta}\end{bmatrix}\\ &= \begin{bmatrix}\dot{\alpha}\cos(\beta) - \dot{\delta}\cos(\alpha)\sin(\beta)\\ \dot{\beta} + \dot{\delta}\sin(\alpha)\\ \dot{\alpha}\sin(\beta) + \dot{\delta}\cos(\alpha)\cos(\beta)\end{bmatrix}.\end{aligned} \tag{21}$$

The pendulum's velocity vector comprises four velocity components, which are the longitudinal lean angular velocity $\dot{\beta}$, the lean angular velocity $\dot{\alpha}$, the pendulum angular velocity $\dot{\gamma}$ and the turning velocity $\dot{\delta}$. These four velocity components are expressed in different coordinate frames, so they are first mapped into the frame Σ_p and the pendulum's velocity vector with respect to the frame Σ_p, Ω_p, is given by:

$$\begin{aligned}\Omega_p &= \begin{bmatrix}\dot{\gamma}\\ 0\\ 0\end{bmatrix} + {}^{p}_{c}T \times \begin{bmatrix}0\\ \dot{\beta}\\ 0\end{bmatrix} + {}^{p}_{w2}T \times \begin{bmatrix}\dot{\alpha}\\ 0\\ 0\end{bmatrix}\\ &\quad + {}^{p}_{g}T \times \begin{bmatrix}0\\ 0\\ \dot{\delta}\end{bmatrix}\\ &= \begin{bmatrix}\dot{\gamma}\\ 0\\ 0\end{bmatrix} + {}^{c}_{p}T^{-1} \times \begin{bmatrix}0\\ \dot{\beta}\\ 0\end{bmatrix} + {}^{w2}_{p}T^{-1} \times \begin{bmatrix}\dot{\alpha}\\ 0\\ 0\end{bmatrix}\\ &\quad + {}^{g}_{p}T^{-1} \times \begin{bmatrix}0\\ 0\\ \dot{\delta}\end{bmatrix}\\ &= \begin{bmatrix}\dot{\gamma} + \dot{\alpha}\cos(\beta) - \dot{\delta}\cos(\alpha)\sin(\beta)\\ \omega_{p2}\\ \omega_{p3}\end{bmatrix},\end{aligned} \tag{22}$$

https://doi.org/10.1017/S0263574715000703 Published online by Cambridge University Press

where

- $\omega_{p2} = \dot{\beta}\cos(\gamma) + \dot{\alpha}\sin(\beta)\sin(\gamma) + \dot{\delta}\sin(\alpha)\cos(\gamma) + \dot{\delta}\cos(\alpha)\cos(\beta)\sin(\gamma)$
- $\omega_{p3} = -\dot{\beta}\sin(\gamma) + \dot{\alpha}\sin(\beta)\cos(\gamma) - \dot{\delta}\sin(\alpha)\sin(\gamma) + \dot{\delta}\cos(\alpha)\cos(\beta)\cos(\gamma)$.

2.5.4. Potential energies & kinetic energies. With the information on the position vectors, linear velocity vectors and angular velocity vectors, the kinetic energy and potential energy for each body can be computed by the following standard formulae from mechanics:

- kinetic energy T_w and potential energy P_w of the wheel:

$$T_w = \frac{1}{2} m_w V_w^T V_w + \frac{1}{2} \Omega_w^T I_w \Omega_w \tag{23}$$

$$P_w = m_w g P_w(3), \tag{24}$$

- kinetic energy T_c and potential energy P_c of the chassis:

$$T_c = \frac{1}{2} m_c V_c^T V_c + \frac{1}{2} \Omega_c^T I_c \Omega_c \tag{25}$$

$$P_c = m_c g P_c(3), \tag{26}$$

- kinetic energy T_p and potential energy P_p of the pendulum:

$$T_p = \frac{1}{2} m_p V_p^T V_p + \frac{1}{2} \Omega_p^T I_p \Omega_p \tag{27}$$

$$P_p = m_p g P_p(3), \tag{28}$$

where $P_w(3)$, $P_c(3)$ and $P_p(3)$ are the third elements of the position vectors P_w, P_c and P_p respectively and they represent the heights of the centers of mass of the wheel, chassis and pendulum from the ground. The total kinetic energy and potential energies of the whole system are the algebraic summations of each body's kinetic energy and potential energy respectively.

- Total kinetic energy T_{total} of the system:

$$T_{total} = T_w + T_c + T_p. \tag{29}$$

- Total potential energy P_{total} of the system:

$$P_{total} = P_w + P_c + P_p. \tag{30}$$

2.5.5. Dynamic model. With the total kinetic and potential energies at hand, we are ready to solve the Lagrange equation (Eq. (5)). First, we compute the Lagrangian (Eq. (6)) using Eqs. (29) and (30). Next, we determine the variables q_i, Q_i and a_{ki}, and the constants n and m. Since there are seven generalized coordinates and two kinematic constraints:

$$m = 7, n = 2.$$

The variables q_i and Q_i, and the constant a_{ki} are given in Table II. If q_1–q_7, Q_1–Q_7, a_{11}–a_{17} and a_{21}–a_{27} are substituted into Eq. (5), the dynamic model is, therefore, expressed by the following seven ordinary differential equations.

$$\frac{d}{dt}\left(\frac{\partial L}{\partial \dot{x}}\right) - \frac{\partial L}{\partial x} = \lambda_1 \tag{31}$$

https://doi.org/10.1017/S0263574715000703 Published online by Cambridge University Press

Table II. The variables for the lagrange equation.

i	q_i	Q_i	a_{1i}	a_{2i}
1	x	0	1	0
2	y	0	0	1
3	θ	τ_w	$-r_w \cos(\delta)$	$-r_w \sin(\delta)$
4	α	0	0	0
5	β	$-\tau_w$	0	0
6	γ	τ_p	0	0
7	δ	0	0	0

$$\frac{d}{dt}\left(\frac{\partial L}{\partial \dot{y}}\right) - \frac{\partial L}{\partial y} = \lambda_2 \tag{32}$$

$$\frac{d}{dt}\left(\frac{\partial L}{\partial \dot{\theta}}\right) - \frac{\partial L}{\partial \theta} = \tau_w - r_w \cos(\delta)\lambda_1 - r_w \sin(\delta)\lambda_2 \tag{33}$$

$$\frac{d}{dt}\left(\frac{\partial L}{\partial \dot{\beta}}\right) - \frac{\partial L}{\partial \beta} = -\tau_w \tag{34}$$

$$\frac{d}{dt}\left(\frac{\partial L}{\partial \dot{\alpha}}\right) - \frac{\partial L}{\partial \alpha} = 0 \tag{35}$$

$$\frac{d}{dt}\left(\frac{\partial L}{\partial \dot{\gamma}}\right) - \frac{\partial L}{\partial \gamma} = \tau_p \tag{36}$$

$$\frac{d}{dt}\left(\frac{\partial L}{\partial \dot{\delta}}\right) - \frac{\partial L}{\partial \delta} = 0. \tag{37}$$

By substituting the Lagrangian into Eqs. (31)–(37) and performing the necessary differentiations and partial differentiations, the seven ordinary differential equations above completely describe the ALP Cycle's dynamics. However, Lagrange multipliers λ_1 and λ_2 in the Eq. (33) can be substituted by their expressions given by Eqs. (31) and (32). Therefore, only five equations remain and this set of ordinary differential equations, shown below, completely describes the robot dynamics.

- Wheel dynamics:

$$\begin{aligned} &m_{11}\ddot{\beta} + m_{12}\ddot{\gamma} + m_{13}\ddot{\delta} + m_{14}\ddot{\theta} + c_{11}\dot{\beta}^2 + c_{12}\dot{\gamma}^2 \\ &\quad + c_{13}\dot{\delta}^2 + c_{14}\dot{\alpha}\dot{\delta} + c_{15}\dot{\beta}\dot{\gamma} + c_{16}\dot{\beta}\dot{\delta} + c_{17}\dot{\gamma}\dot{\delta} = \tau_w. \end{aligned} \tag{38}$$

- Chassis longitudinal dynamics:

$$\begin{aligned} &m_{21}\ddot{\alpha} + m_{22}\ddot{\beta} + m_{23}\ddot{\delta} + m_{24}\ddot{\theta} + c_{21}\dot{\alpha}^2 + c_{22}\dot{\delta}^2 + c_{23}\dot{\alpha}\dot{\gamma} \\ &\quad + c_{24}\dot{\alpha}\dot{\delta} + c_{25}\dot{\beta}\dot{\gamma} + c_{26}\dot{\gamma}\dot{\delta} + c_{27}\dot{\delta}\dot{\theta} + g_{21} = -\tau_w. \end{aligned} \tag{39}$$

- Chassis lateral dynamics:

$$\begin{aligned} &m_{31}\ddot{\alpha} + m_{32}\ddot{\beta} + m_{33}\ddot{\gamma} + m_{34}\ddot{\delta} + c_{31}\dot{\beta}^2 + c_{32}\dot{\gamma}^2 + c_{33}\dot{\delta}^2 \\ &\quad + c_{34}\dot{\alpha}\dot{\beta} + c_{35}\dot{\alpha}\dot{\gamma} + c_{36}\dot{\beta}\dot{\gamma} + c_{37}\dot{\beta}\dot{\delta} + c_{38}\dot{\gamma}\dot{\delta} + c_{39}\dot{\delta}\dot{\theta} = 0. \end{aligned} \tag{40}$$

https://doi.org/10.1017/S0263574715000703 Published online by Cambridge University Press

■ Pendulum dynamics:

$$\begin{aligned} & m_{41}\ddot{\alpha} + m_{42}\ddot{\gamma} + m_{43}\ddot{\delta} + m_{44}\ddot{\theta} + c_{41}\dot{\alpha}^2 + c_{42}\dot{\beta}^2 + c_{43}\dot{\delta}^2 \\ & \quad + \ c_{44}\dot{\alpha}\dot{\beta} + c_{45}\dot{\alpha}\dot{\delta} + c_{46}\dot{\beta}\dot{\delta} + c_{47}\dot{\delta}\dot{\theta} + g_{41} = \tau_p. \end{aligned} \tag{41}$$

■ Turning dynamics:

$$\begin{aligned} & m_{51}\ddot{\alpha} + m_{52}\ddot{\beta} + m_{53}\ddot{\gamma} + m_{54}\ddot{\delta} + m_{55}\ddot{\theta} + c_{51}\dot{\alpha}^2 + c_{52}\dot{\beta}^2 \\ & \quad + \ c_{53}\dot{\gamma}^2 + c_{54}\dot{\alpha}\dot{\beta} + c_{55}\dot{\alpha}\dot{\gamma} + c_{56}\dot{\alpha}\dot{\delta} + c_{57}\dot{\alpha}\dot{\theta} + c_{58}\dot{\beta}\dot{\gamma} \\ & \quad + \ c_{59}\dot{\beta}\dot{\delta} + c_{510}\dot{\gamma}\dot{\delta} + c_{511}\dot{\delta}\dot{\theta} = 0. \end{aligned} \tag{42}$$

The dynamic model shown above is just a brief presentation. The complete description of the coefficients m_{11}–m_{55}, c_{11}–c_{511} and g_{21}–g_{41} can be requested from the authors. These coefficients are functions of the angular positions, physical parameters and environmental parameter. Therefore, this dynamic model is nonlinear.

3. Model Simplification

The ALP Cycle's dynamic model, derived in Section 2, is too large and complex for analysis and control design. Therefore, it is simplified by pseudolinearization with respect to the upright equilibrium posture of the robot. This posture is described by the following conditions.

$$\alpha = \beta = \gamma = 0^\circ \tag{43}$$

$$\dot{\alpha} = \dot{\beta} = \dot{\gamma} = 0^\circ/s. \tag{44}$$

The pseudolinearization is performed by executing the following steps.

■ *Step 1*: Approximate the sines of α, β and γ by their respective angles, that is

$$\sin(\alpha) \approx \alpha, \sin(\beta) \approx \beta, \sin(\gamma) \approx \gamma.$$

■ *Step 2*: Approximate the cosines of α, β and γ by 1, that is

$$\cos(\alpha) \approx 1, \cos(\beta) \approx 1, \cos(\gamma) \approx 1.$$

■ *Step 3*: Eliminate the second-order and higher-order terms in the dynamic model and its coefficients m_{11}–m_{55}, c_{11}–c_{511} and g_{21}–g_{41}.

The application of *Step 1* until *Step 3* to Eqs. (38)–(42) results in the following simplified dynamic model:

■ Wheel dynamics:

$$\begin{aligned} & \epsilon_1 r_w\ddot{\beta} + (I_{w2} + \epsilon_3 r_w + \epsilon_1 r_w)\alpha\ddot{\delta} + \epsilon_2 r_w\gamma\ddot{\delta} + (I_{w2} \\ & \quad + \ \epsilon_3 r_w)\ddot{\theta} - \epsilon_1 r_w\beta\dot{\delta}^2 + (I_{w2} + 2\epsilon_3 r_w + 2\epsilon_1 r_w)\dot{\alpha}\dot{\delta} \\ & \quad + \ 2\epsilon_2 r_w\dot{\gamma}\dot{\delta} = \tau_w. \end{aligned} \tag{45}$$

https://doi.org/10.1017/S0263574715000703 Published online by Cambridge University Press

■ Chassis longitudinal dynamics:

$$\begin{aligned}&(I_{c2}+I_{p2}+\rho_1)\ddot{\beta}+(I_{c2}+I_{p2}+\rho_1+\epsilon_1 r_w)\alpha\ddot{\delta}+(\sigma_3\\&\quad+\ \rho_3)\gamma\ddot{\delta}+\epsilon_1 r_w\ddot{\theta}-(\sigma_4+\rho_1)\beta\dot{\delta}^2+(I_{c1}+\sigma_2+I_{p1}\\&\quad+\ \sigma_3+2\rho_1+2\epsilon_1 r_w)\dot{\alpha}\dot{\delta}+(I_{p1}+\sigma_3+2\rho_3)\dot{\gamma}\dot{\delta}-\epsilon_1 g\beta\\&=-\tau_w.\end{aligned}\tag{46}$$

■ Chassis lateral dynamics:

$$\begin{aligned}&(I_{w1}+I_{c1}+I_{p1}+\epsilon_3 r_w+\rho_1+2\epsilon_1 r_w)\ddot{\alpha}+(I_{p1}+\epsilon_2 r_w\\&\quad+\ \rho_3)\ddot{\gamma}-(\sigma_4+\epsilon_1 r_w+\rho_1)\beta\ddot{\delta}-(\sigma_1+\sigma_2+\sigma_3+\epsilon_3 r_w\\&\quad+\ \rho_1+2\epsilon_1 r_w)\alpha\dot{\delta}^2-(\sigma_3+\rho_3+\epsilon_2 r_w)\gamma\dot{\delta}^2-(I_{c1}+\sigma_2\\&\quad+\ I_{p1}+\sigma_3+2\rho_1+2\epsilon_1 r_w)\dot{\beta}\dot{\delta}-(I_{w2}+\epsilon_3 r_w\\&\quad+\ \epsilon_1 r_w)\dot{\delta}\dot{\theta}-(\epsilon_3+\epsilon_1)g\alpha-\epsilon_2 g\gamma=0.\end{aligned}\tag{47}$$

■ Pendulum dynamics:

$$\begin{aligned}&(I_{p1}+\epsilon_2 r_w+\rho_3)\ddot{\alpha}+(I_{p1}+\epsilon_2 l_p)\ddot{\gamma}-(I_{p1}+\rho_3)\beta\ddot{\delta}\\&\quad-\ (\sigma_3+\epsilon_2 r_w+\rho_3)\alpha\dot{\delta}^2-(\sigma_3+\epsilon_2 l_p)\gamma\dot{\delta}^2-(I_{p1}+\sigma_3\\&\quad+\ 2\rho_3)\dot{\beta}\dot{\delta}-\epsilon_2 r_w\dot{\delta}\dot{\theta}-\epsilon_2 g\alpha-\epsilon_2 g\gamma=\tau_p.\end{aligned}\tag{48}$$

■ Turning dynamics:

$$\begin{aligned}&-(\sigma_4+\rho_1+\epsilon_1 r_w)\beta\ddot{\alpha}+(I_{c2}+I_{p2}+\rho_1+\epsilon_1 r_w)\alpha\ddot{\beta}\\&\quad+\ (\sigma_3+\rho_3)\gamma\ddot{\beta}-(I_{p1}+\rho_3)\beta\ddot{\gamma}+(I_{w3}+I_{c3}+I_{p3})\ddot{\delta}\\&\quad+\ (I_{w2}+\epsilon_3 r_w+\epsilon_1 r_w)\alpha\ddot{\theta}+\epsilon_2 r_w\gamma\ddot{\theta}+I_{w2}\dot{\alpha}\dot{\theta}\\&\quad+\ \epsilon_1 r_w\beta\dot{\delta}\dot{\theta}=0.\end{aligned}\tag{49}$$

where $\epsilon_1=m_c l_c+m_p(l_c+l_{cp}+l_p)$, $\epsilon_2=m_p l_p$, $\epsilon_3=(m_w+m_c+m_p)r_w$, $\rho_1=m_c l_c^2+m_p(l_c+l_{cp}+l_p)^2$, $\rho_2=m_p l_p^2$, $\rho_3=m_p(l_c+l_{cp}+l_p)l_p$, $\sigma_1=I_{w2}-I_{w3}$, $\sigma_2=I_{c2}-I_{c3}$, $\sigma_3=I_{p2}-I_{p3}$, $\sigma_4=I_{c1}-I_{c3}+I_{p1}-I_{p3}$. It can be seen that, although the simplified dynamic model is linear with respect to α, β, γ, $\ddot{\alpha}$, $\ddot{\beta}$, $\ddot{\gamma}$, $\dot{\alpha}$, $\dot{\beta}$ and $\dot{\gamma}$, it is still nonlinear with respect to δ, θ, $\dot{\delta}$, $\dot{\theta}$, $\ddot{\delta}$ and $\ddot{\theta}$.

This simplified model is used in Section 4 to study the ALP Cycle's characteristics and derive some formulae useful for the control design.

4. Robot Characteristics

Based on the dynamic model and its simplified version, the characteristics of the ALP Cycle's dynamics can be properly investigated. This investigation is very important for the fundamental understanding of the robot's behaviors and useful for the control design and prototype improvement.

4.1. Mode separation

The dynamics of the ALP Cycle can largely be separated into three modes which are (1) longitudinal mode, (2) lateral mode and (3) turning mode. This separation is based on the motion which each submodel largely represents. Due to the large scale and high complexity of the robot model, detailed study is very cumbersome. In this respect, the mode separation makes analysis and investigation much simpler and more manageable.

https://doi.org/10.1017/S0263574715000703 Published online by Cambridge University Press

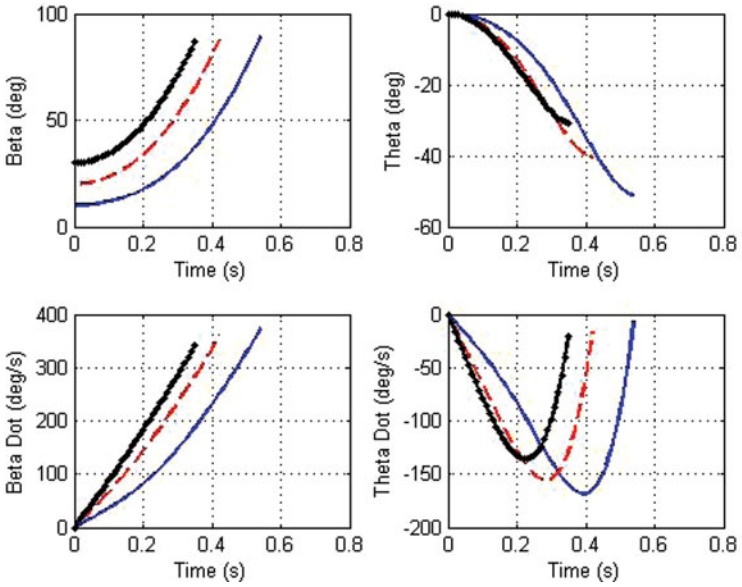


Fig. 4. The open-loop responses to static non-upright longitudinal initial postures.

The *longitudinal mode* or *pitch mode* consists of the wheel dynamics (Eq. (38)) and the chassis longitudinal dynamics (Eq. (39)). This mode describes the robot motion in the longitudinal or pitch or forward–backward direction. It can also be called *Single-Wheeled Inverted Pendulum mode* because its dominant dynamics are essentially the dynamics of the Single-Wheeled Inverted Pendulum,[4].[10] The longitudinal mode can be directly controlled by the wheel torque τ_w.

The *lateral mode* or *roll mode* comprises the chassis lateral dynamics (Eq. (40)) and the pendulum dynamics (Eq. (41)). It describes the motion of the ALP Cycle in the lateral or roll or left-right direction. This mode can also be called *Acrobot mode* because its dominant dynamics are essentially the dynamics of the Acrobot,[4].[5] The lateral mode can be directly controlled by the pendulum torque τ_p.

The *turning mode* or *yaw mode* is only made up of the turning dynamics (Eq. (42)). This mode describes the robot motion in the turning or yaw direction. Unlike the longitudinal and lateral modes, the turning mode does not have a direct control input, so its control must be approached indirectly by the coordinated control of the wheel torque and the pendulum torque.

4.2. Open-loop responses

We perform three cases of numerical simulations in MATLAB in order to understand the open-loop responses of the ALP Cycle when released from a static non-upright initial posture. The general posture of the ALP Cycle is defined only by the variables α, β and γ. Therefore, all other variables are set to zero. In all three cases, the explicit Runge–Kutta (4, 5) formula, the Dormand–Prince pair, coded in MATLAB *ode45* function, is used to solve the ordinary differential equations involved. The parameters given in Table I are used in the simulations.

4.2.1. Static non-upright longitudinal initial postures. In the first case, we use three initial postures which are:

(1) $\beta = 10^\circ, \alpha = 0^\circ, \gamma = 0^\circ$
(2) $\beta = 20^\circ, \alpha = 0^\circ, \gamma = 0^\circ$
(3) $\beta = 30^\circ, \alpha = 0^\circ, \gamma = 0^\circ$

and set all control inputs to zero. The simulation results are shown in Fig. 4.

The simulation results show that, without active control, the longitudinal mode is unstable. It can be observed that the three initial postures grow exponentially and, with smaller initial posture, the time taken for the ALP Cycle to fall down is longer.

https://doi.org/10.1017/S0263574715000703 Published online by Cambridge University Press

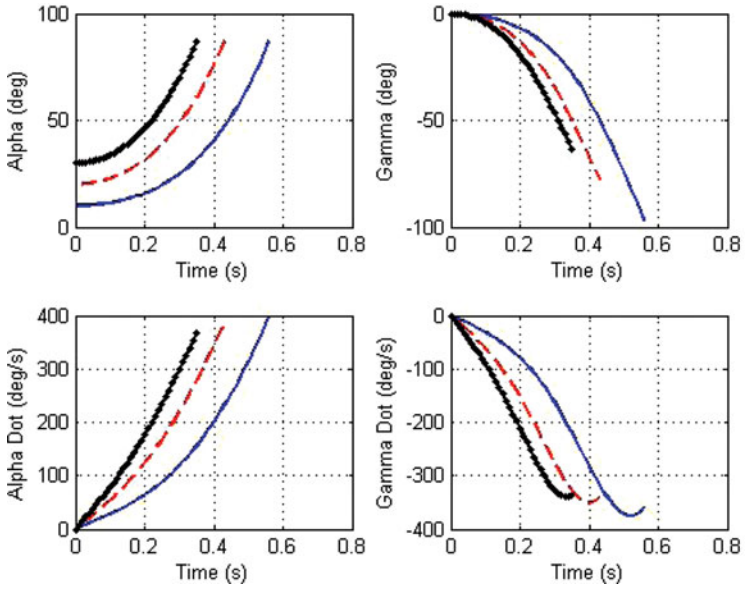


Fig. 5. The open-loop responses to static non-upright lateral initial postures.

4.2.2. Static non-upright lateral initial postures. In the second case, we use three initial postures which are:

(1) $\beta = 0^\circ, \alpha = 10^\circ, \gamma = 0^\circ$
(2) $\beta = 0^\circ, \alpha = 20^\circ, \gamma = 0^\circ$
(3) $\beta = 0^\circ, \alpha = 30^\circ, \gamma = 0^\circ$

and set all control inputs to zero. The simulation results are shown in Fig. 5.

Similar with the first case, the simulation results in the second case show that, without active control, the lateral mode is unstable. It can be observed that the three initial postures grow exponentially and, with smaller initial posture, the time taken for the ALP Cycle to fall down is longer.

4.2.3. Static non-upright mixed initial postures. In the third case, we use the following three initial postures:

(1) $\beta = 10^\circ, \alpha = 10^\circ, \gamma = 0^\circ$
(2) $\beta = 10^\circ, \alpha = 20^\circ, \gamma = 0^\circ$
(3) $\beta = 10^\circ, \alpha = 30^\circ, \gamma = 0^\circ$

and set all the control inputs to zero. The simulation results are shown in Figs. 6 and 7.

The simulation results show that as the ALP Cycle falls down in two directions, the turning angle changes. This fact shows that the turning mode is controllable through the longitudinal and lateral modes.

4.3. Equilibrium

It is obvious that the upright posture is an equilibrium point of the ALP Cycle, but it is not the only one. We can find the other equilibrium points by investigating the resulting dynamic models when the ALP Cycle is constrained to move only in the longitudinal and lateral directions.

When the ALP Cycle is constrained to move only in the longitudinal direction, its dynamic model can be simplified as followed.

https://doi.org/10.1017/S0263574715000703 Published online by Cambridge University Press

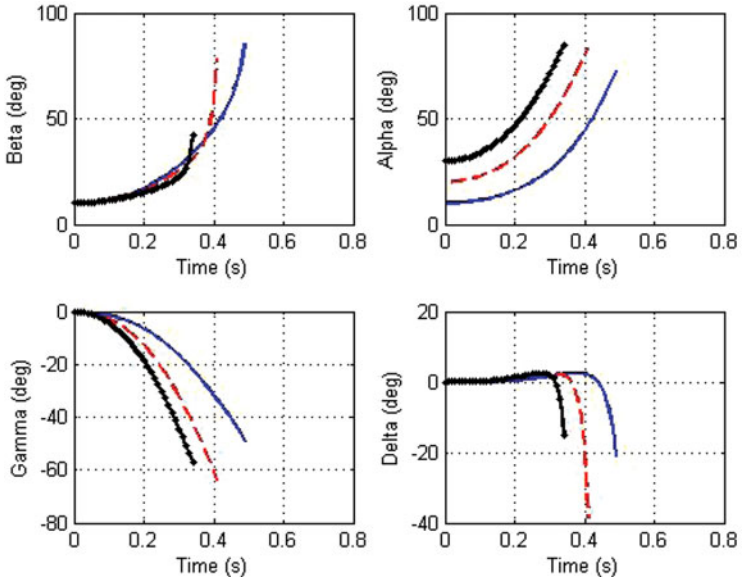


Fig. 6. The open-loop responses to static non-upright mixed initial postures.

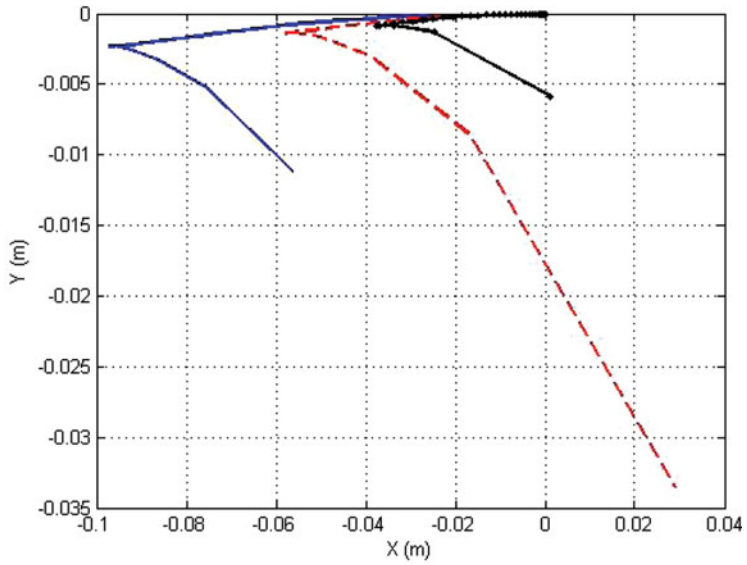


Fig. 7. The open-loop responses to static non-upright mixed initial postures.

■ Wheel dynamics:

$$\left[\frac{I_{w2}}{r_w}^2 + (m_w + m_c + m_p)r_w^2\right]\ddot{\theta} + [m_c l_c + m_p(l_c + l_{cp} + l_p)]r_w \cos(\beta)\ddot{\beta} - [m_c l_c + m_p(l_c + l_{cp} + l_p)]r_w \sin(\beta)\dot{\beta}^2 = \tau_w. \tag{50}$$

■ Chassis longitudinal dynamics:

$$[m_c l_c + m_p(l_c + l_{cp} + l_p)]r_w \cos(\beta)\ddot{\theta} + [I_{c2} + I_{p2} + m_c l_c^2 + m_p(l_c + l_{cp} + l_p)^2]\ddot{\beta} - [m_c l_c + m_p(l_c + l_{cp} + l_p)]\sin(\beta)g = -\tau_w. \tag{51}$$

https://doi.org/10.1017/S0263574715000703 Published online by Cambridge University Press

At equilibrium, $\ddot{\beta} = \ddot{\theta} = 0$ and $\dot{\beta} = 0$. Substituting these conditions into Eqs. (50) and (51) results in two solutions (1) $\beta = 0^\circ$, $\tau_w = 0\ N \cdot m$ and (2) $\beta = 180^\circ$, $\tau_w = 0\ N \cdot m$. However, because the chassis and pendulum are never below the wheel, the second equilibrium point is not considered. Therefore, the upright posture is the only equilibrium point of the longitudinal mode.

When the ALP Cycle is constrained to move only in the lateral direction, its dynamic model can be reduced to the following equations.

- Chassis lateral dynamics:

$$\begin{aligned}
&[I_{w1} + I_{c1} + I_{p1} + m_w r_w^2 + m_c(r_w + l_c)^2 + m_p(r_w \\
&\quad + l_c + l_{cp})^2 + m_p l_p^2 + 2m_p(r_w + l_c + l_{cp}) l_p \cos(\gamma)]\ddot{\alpha} \\
&\quad + [I_{p1} + m_p l_p^2 + m_p(r_w + l_c + l_{cp}) l_p \cos(\gamma)]\ddot{\gamma} \\
&\quad - 2m_p(r_w + l_c + l_{cp}) l_p \sin(\gamma)\dot{\alpha}\dot{\gamma} - m_p(r_w + l_c \\
&\quad + l_{cp}) l_p \sin(\gamma)\dot{\gamma}^2 - (m_w r_w + m_c(r_w + l_c) + m_p(r_w \\
&\quad + l_c + l_{cp})) \sin(\alpha) g - m_p l_p \sin(\alpha + \gamma) g = 0.
\end{aligned} \tag{52}$$

- Pendulum dynamics:

$$\begin{aligned}
&[I_{p1} + m_p l_p^2 + m_p(r_w + l_c + l_{cp}) l_p \cos(\gamma)]\ddot{\alpha} + (I_{p1} \\
&\quad + m_p l_p^2)\ddot{\gamma} + m_p(r_w + l_c + l_{cp}) l_p \sin(\gamma)\dot{\alpha}^2 \\
&\quad - m_p l_p \sin(\alpha + \gamma) g = \tau_p.
\end{aligned} \tag{53}$$

At equilibrium, $\ddot{\alpha} = \ddot{\gamma} = 0$ and $\dot{\alpha} = \dot{\gamma} = 0$. Substituting these conditions into Eqs. (52) and (53) results in the following two equations.

$$\begin{aligned}
&- (m_w r_w + m_c(r_w + l_c) + m_p(r_w + l_c + l_{cp})) \sin(\alpha) g \\
&\quad - m_p l_p \sin(\alpha + \gamma) g = 0
\end{aligned} \tag{54}$$

$$-m_p l_p \sin(\alpha + \gamma) g = \tau_p. \tag{55}$$

Equation (54) represents the relationship between α and γ at equilibrium and can be expressed more explicitly as:

$$\gamma = \sin^{-1}\left(-\frac{c_1 \alpha}{c_2}\right) - \alpha, \tag{56}$$

where

$$c_1 = m_w r_w + m_c(r_w + l_c) + m_p(r_w + l_c + l_{cp})$$

$$c_2 = m_p l_p.$$

For any α such that the magnitude of the argument of the inverse sine in Eq. (56) does not exceed 1, there always exists the corresponding γ. So, the equilibrium of the lateral mode is a continuum instead of an isolated point. Equation (55) gives the control input at a specific equilibrium point in the continuum.

In short, the ALP Cycle has an isolated equilibrium point in the longitudinal direction and an equilibrium continuum in the lateral direction. Combining these two observations, it can be concluded that the equilibrium of the ALP Cycle is a continuum described by Eq. (56) at $\beta = 0^\circ$.

https://doi.org/10.1017/S0263574715000703 Published online by Cambridge University Press

4.4. Lateral-statics boundary & lateral-statics constant

Further insight can be gained from Eq. (56). For γ to be defined, the absolute value of the argument of the inverse sine in Eq. (56) must always be less than or equal to 1. Therefore, the magnitude of α is bounded by

$$|-\frac{c_1|\alpha|}{c_2}| = \frac{c_1|\alpha|}{c_2} \leq 1 \Rightarrow |\alpha| \leq \frac{c_2}{c_1} = K_{lsb}. \tag{57}$$

K_{lsb} is called *lateral-statics boundary* because it defines the largest lean angle α such that equilibrium is still physically achievable.

If α and γ are sufficiently small, Eq. (56) can be simplified to

$$\gamma = -\left(1 + \frac{c_1}{c_2}\right)\alpha = K_{ls}\alpha. \tag{58}$$

K_{ls} is named *lateral-statics constant* and can be written in a more insightful form as

$$K_{ls} = -1 - \frac{m_w r_w + m_c(r_w + l_c)}{m_p l_p} - \frac{r_w + l_c + l_{cp}}{l_p}. \tag{59}$$

When the balancing or steering of the ALP Cycle using linear controllers is concerned, it is desirable to limit the posture in the vicinity of the upright posture. However, Eq. (58) shows that γ is the product of α and K_{ls}. It means that small α does not guarantee γ to be small. It is clearly desireable to have as small K_{ls} as possible so that small α translates into small γ. From Eq. (59), it can be seen that

$$inf(|K_{ls}|) = 1,$$

and this happens when the second and third terms in Eq. (59) equal to zero. To achieve this, l_p must be made as large as possible in comparison with the other ALP Cycle's physical parameters and m_p should not be small (i.e. the pendulum should be extremely long and must not be light).

Equation (55) gives the pendulum torque τ_p required to maintain the balanced posture, either upright or non-upright. For sufficiently small α and γ, it can be written as

$$\tau_p = m_p l_p g(\alpha + \gamma).$$

The maximum value of the magnitude of the pendulum torque is

$$max(|\tau_p|) = m_p l_p g. \tag{60}$$

Relating Eq. (60) and the previous discussion, it is clear that small K_{ls} can only be achieved at the expense of large τ_p. In practice, large τ_p is undesirable as it means that bigger and more powerful motor is needed. Therefore, trade-off is unavoidable and, as far as practical application is concerned, with the available motor size and power in the market, K_{ls} can only be reduced to a certain value, but it will never reach 1 and this means, as long as linear controllers are used, the practical ALP Cycle prototype can only operate successfully at very small range of angles in the vicinity of its upright equilibrium posture.

Based on the parameters in Table I, the lateral-statics boundary K_{lbs} and the lateral-statics constant K_{ls} of the constructed ALP Cycle prototype are 8.08° and -8.12 respectively.

4.5. Turning constant & path curvature

In order to find out the way of controlling the turning motion, we refer to Eq. (49). If the forward acceleration is sufficiently small and perfect set-point control of forward speed is achieved, then the forward speed of ALP Cycle is constant and equal to its reference V_{ref}. In addition, the longitudinal lean angle β is zero. Furthermore, if the second derivatives of α, β and γ are sufficiently small, then

https://doi.org/10.1017/S0263574715000703 Published online by Cambridge University Press

they can safely be ignored. Therefore, the following conditions apply:

$$\ddot{\alpha} = \ddot{\beta} = \ddot{\gamma} = 0$$

$$\ddot{\theta} = 0, \dot{\theta} = \frac{V_{ref}}{r_w}, \beta = 0$$

which reduce Eq. (49) into the following equation:

$$\ddot{\delta} = -\frac{I_{w2} V_{ref}}{(I_{w3} + I_{c3} + I_{p3}) r_w} \dot{\alpha} = K_{turn} V_{ref} \dot{\alpha}. \tag{61}$$

K_{turn} in Eq. (61) is named *turning constant*. Both sides of Eq. (61) can be integrated to get:

$$\dot{\delta}(t) = \dot{\delta}(t_0) + K_{turn} V_{ref} [\alpha(t) - \alpha(t_0)], \tag{62}$$

which shows that the turning speed $\dot{\delta}$ is linearly dependent on lateral lean angle α for a given constant forward speed V_{ref}.

If the ALP Cycle is arranged to start its motion from its upright balanced configuration, $\dot{\delta}(t_0)$ and $\alpha(t_0)$ are zero. In this case, Eq. (62) becomes:

$$\dot{\delta}(t) = K_{turn} V_{ref} \alpha(t). \tag{63}$$

An important point can be inferred from Eq. (63). For a certain constant forward speed, for the ALP Cycle to turn faster, it has to lean more. However, if the applied controller is linear controller, larger lateral lean angle means that the system may leave its linear region and, hence, the stability of the system can no longer be guaranteed. Therefore, the ALP Cycle's turning speed is limited by how far the ALP Cycle can lean sidewards without compromising its stability. This limit can be expressed by the following equation.

$$max(|\dot{\delta}(t)|) = K_{turn} V_{ref} max(|\alpha|). \tag{64}$$

Based on the parameters in Table I, the turning constant K_{turn} of the constructed ALP Cycle prototype is $-1.48/\text{m}$.

When the ALP Cycle performs circling motion, its forward speed is related to its turning speed by

$$V_{ref} = R_p \dot{\delta}, \tag{65}$$

where R_p is the radius of curvature of the path traversed by the robot. Substituting $\dot{\delta}$ from Eq. (63) into Eq. (65), the radius of path curvature is given by:

$$R_p = \frac{1}{K_{turn} \alpha} \tag{66}$$

in which the sign of R_p simply determines the path heading. Positive R_p means that, with a certain forward speed, the path heads in the direction of positive δ and vice versa. Equation (66) implies that smaller radius of curvature or sharper turning requires larger lean angle. If the maximum lean angle for a certain applied control law under which the system's stability can still be maintained is $|\alpha|_{max}$, then the minimum radius of curvature is

$$|R_p|_{min} = \frac{1}{K_{turn} |\alpha|_{max}}. \tag{67}$$

With the turning constant K_{turn} given previously and the assumption that we implement a control law capable of controlling α to the its maximum achievable limit expressed by the lateral-statics boundary K_{lsb} the minimum magnitude of the path radius of curvature is 4.79 m.

https://doi.org/10.1017/S0263574715000703 Published online by Cambridge University Press

4.6. State-space forms & coupling disturbances

Referring to the simplified models of the longitudinal, lateral and turning dynamics (Eqs. (45)–(49)), if seen carefully, it can be observed that these three dynamics contain some perturbations coming from the couplings among themselves. In order to make it more obvious, each mode needs to be put into state-space minimum-realization form.

The longitudinal dynamics (Eqs. (45) and (46)) can be put into the following state-space form:

$$\dot{x}_{long} = A_{long}(\dot{\delta})x_{long} + B_{long}\tau_w + W_{long}(\alpha, \gamma, \dot{\delta}, \dot{\alpha}, \dot{\gamma}, \ddot{\delta}), \tag{68}$$

where

- $x_{long} = \begin{bmatrix} \beta & \dot{\beta} & \dot{\theta} \end{bmatrix}^T$
- $A_{long}(\dot{\delta}) = \begin{bmatrix} 0 & 1 & 0 \\ a_{long21} & 0 & 0 \\ a_{long31} & 0 & 0 \end{bmatrix}$
- $a_{long21} = \frac{[\epsilon_1^2 r_w^2 - (I_{w2}+\epsilon_3 r_w)(\sigma_4+\rho_1)]}{d_{long}}\dot{\delta}^2 - \frac{(I_{w2}+\epsilon_3 r_w)\epsilon_1 g}{d_{long}}$
- $a_{long31} = \frac{[-\epsilon_1 r_w(I_{c2}+I_{p2}+\rho_1)+(\sigma_4+\rho_1)\epsilon_1 r_w]}{d_{long}}\dot{\delta}^2 + \frac{\epsilon_1^2 r_w g}{d_{long}}$
- $B_{long} = \begin{bmatrix} 0 \\ \frac{\epsilon_1 r_w + I_{w2} + \epsilon_3 r_w}{d_{long}} \\ \frac{-I_{c2} - I_{p2} - \rho_1 - \epsilon_1 r_w}{d_{long}} \end{bmatrix}$
- $W_{long}(\alpha, \gamma, \dot{\delta}, \dot{\alpha}, \dot{\gamma}, \ddot{\delta}) = \begin{bmatrix} 0 \\ w_{long2} \\ w_{long3} \end{bmatrix}$
- $w_{long2} = \frac{1}{d_{long}}\{[-(I_{w2} + \epsilon_3 r_w + \epsilon_1 r_w)\epsilon_1 r_w + (I_{w2} + \epsilon_3 r_w)(I_{c2} + I_{p2} + \rho_1 + \epsilon_1 r_w)]\alpha\ddot{\delta} + [-\epsilon_2\epsilon_1 r_w^2 + (\sigma_3 + \rho_3)(I_{w2} + \epsilon_3 r_w)]\gamma\ddot{\delta} + [-(I_{w2} + 2\epsilon_3 r_w + 2\epsilon_1 r_w)\epsilon_1 r_w + (I_{c1} + \sigma_2 + I_{p1} + \sigma_3 + 2\rho_1 + 2\epsilon_1 r_w)(I_{w2} + \epsilon_3 r_w)]\dot{\alpha}\dot{\delta} + [-2\epsilon_2\epsilon_1 r_w^2 + (I_{p1} + \sigma_3 + 2\rho_3)(I_{w2} + \epsilon_3 r_w)]\dot{\gamma}\dot{\delta}\}$
- $w_{long3} = \frac{1}{d_{long}}\{[(I_{c2} + I_{p2} + \rho_1)(I_{w2} + \epsilon_3 r_w + \epsilon_1 r_w) - (I_{c2} + I_{p2} + \rho_1 + \epsilon_1 r_w)\epsilon_1 r_w]\alpha\ddot{\delta} + [(I_{c2} + I_{p2} + \rho_1)\epsilon_2 r_w - (\sigma_3 + \rho_3)\epsilon_1 r_w]\gamma\ddot{\delta} + [(I_{c2} + I_{p2} + \rho_1)(I_{w2} + 2\epsilon_3 r_w + 2\epsilon_1 r_w) - (I_{c1} + \sigma_2 + I_{p1} + \sigma_3 + 2\rho_1 + 2\epsilon_1 r_w)\epsilon_1 r_w]\dot{\alpha}\dot{\delta} + [(I_{c2} + I_{p2} + \rho_1)2\epsilon_2 r_w - (I_{p1} + \sigma_3 + 2\rho_3)\epsilon_1 r_w]\dot{\gamma}\dot{\delta}\}$
- $d_{long} = \epsilon_1^2 r_w^2 - (I_{w2} + \epsilon_3 r_w)(I_{c2} + I_{p2} + \rho_1)$.

The longitudinal system matrix A_{long} is perturbed by $\dot{\delta}$ and the system is disturbed by W_{long} which is called *longitudinal coupling disturbance*.

The lateral dynamics (Eqs. (47) and (48)) can be put into the following state-space form:

$$\dot{x}_{lat} = A_{lat}(\dot{\delta})x_{lat} + B_{lat}\tau_p + W_{lat}(\beta, \dot{\delta}, \dot{\theta}, \dot{\beta}, \ddot{\delta}), \tag{69}$$

where

- $x_{lat} = \begin{bmatrix} \alpha & \gamma & \dot{\alpha} & \dot{\gamma} \end{bmatrix}^T$
- $A_{lat}(\dot{\delta}) = \begin{bmatrix} 0 & 0 & 1 & 0 \\ 0 & 0 & 0 & 1 \\ a_{lat31} & a_{lat32} & 0 & 0 \\ a_{lat41} & a_{lat42} & 0 & 0 \end{bmatrix}$
- $a_{lat31} = \frac{1}{d_{lat}}\{[(\sigma_1 + \sigma_2 + \sigma_3 + \epsilon_3 r_w + \rho_1 + 2\epsilon_1 r_w)(I_{p1} + \epsilon_2 l_p) - (I_{p1} + \epsilon_2 r_w + \rho_3)(\sigma_3 + \epsilon_2 r_w + \rho_3)]\dot{\delta}^2 + [-(I_{p1} + \epsilon_2 r_w + \rho_3)\epsilon_2 g + (\epsilon_3 + \epsilon_1)g(I_{p1} + \epsilon_2 l_p)]\}$
- $a_{lat32} = \frac{1}{d_{lat}}\{[-(\sigma_3 + \epsilon_2 l_p)(I_{p1} + \epsilon_2 r_w + \rho_3) + (\sigma_3 + \rho_3 + \epsilon_2 r_w)(I_{p1} + \epsilon_2 l_p)]\dot{\delta}^2 + [-(I_{p1} + \epsilon_2 r_w + \rho_3)\epsilon_2 g + \epsilon_2 g(I_{p1} + \epsilon_2 l_p)]\}$

https://doi.org/10.1017/S0263574715000703 Published online by Cambridge University Press

- $a_{lat41} = \frac{1}{d_{lat}}\{[-(I_{p1} + \epsilon_2 r_w + \rho_3)(\sigma_1 + \sigma_2 + \sigma_3 + \epsilon_3 r_w + \rho_1 + 2\epsilon_1 r_w) + (I_{w1} + I_{c1} + I_{p1} + \epsilon_3 r_w + \rho_1 + 2\epsilon_1 r_w)(\sigma_3 + \epsilon_2 r_w + \rho_3)]\dot{\delta}^2 + [(I_{p1} + \epsilon_2 r_w + \rho_3)\epsilon_1)g + (I_{w1} + I_{c1} + I_{p1} + \epsilon_3 r_w + \rho_1 + 2\epsilon_1 r_w)\epsilon_2 g]\}$
- $a_{lat42} = \frac{1}{d_{lat}}\{[-(\sigma_3 + \rho_3 + \epsilon_2 r_w)(I_{p1} + \epsilon_2 r_w + \rho_3) + (\sigma_3 + \epsilon_2 l_p)(I_{w1} + I_{c1} + I_{p1} + \epsilon_3 r_w + \rho_1 + 2\epsilon_1 r_w)]\dot{\delta}^2 + [-\epsilon_2 g(I_{p1} + \epsilon_2 r_w + \rho_3) + \epsilon_2 g(I_{w1} + I_{c1} + I_{p1} + \epsilon_3 r_w + \rho_1 + 2\epsilon_1 r_w)]\}$
- $B_{lat} = \begin{bmatrix} 0 \\ 0 \\ \frac{-(I_{p1}+\epsilon_2 r_w+\rho_3)}{d_{lat}} \\ \frac{(I_{w1}+I_{c1}+I_{p1}+\epsilon_3 r_w+\rho_1+2\epsilon_1 r_w)}{d_{lat}} \end{bmatrix}$
- $W_{lat}(\beta, \dot{\delta}, \dot{\theta}, \dot{\beta}, \ddot{\delta}) = \begin{bmatrix} 0 \\ 0 \\ w_{lat3} \\ w_{lat4} \end{bmatrix}$
- $w_{lat3} = \frac{1}{d_{lat}}\{[-(I_{p1} + \epsilon_2 r_w + \rho_3)(I_{p1} + \rho_3) + (I_{p1} + \epsilon_2 l_p)(\sigma_4 + \epsilon_1 r_w + \rho_1)]\beta\ddot{\delta} + [-(I_{p1} + \epsilon_2 r_w + \rho_3)(I_{p1} + \sigma_3 + 2\rho_3) + (I_{p1} + \epsilon_2 l_p)(I_{c1} + \sigma_2 + I_{p1} + \sigma_3 + 2\rho_1 + 2\epsilon_1 r_w)]\dot{\beta}\dot{\delta} + [-(I_{p1} + \epsilon_2 r_w + \rho_3)\epsilon_2 r_w + (I_{w2} + \epsilon_3 r_w + \epsilon_1 r_w)(I_{p1} + \epsilon_2 l_p)]\dot{\delta}\dot{\theta}\}$
- $w_{lat4} = \frac{1}{d_{lat}}\{[-(I_{p1} + \epsilon_2 r_w + \rho_3)(\sigma_4 + \epsilon_1 r_w + \rho_1) + (I_{w1} + I_{c1} + I_{p1} + \epsilon_3 r_w + \rho_1 + 2\epsilon_1 r_w)(I_{p1} + \rho_3)]\beta\ddot{\delta} + [-(I_{p1} + \epsilon_2 r_w + \rho_3)(I_{c1} + \sigma_2 + I_{p1} + \sigma_3 + 2\rho_1 + 2\epsilon_1 r_w) + (I_{w1} + I_{c1} + I_{p1} + \epsilon_3 r_w + \rho_1 + 2\epsilon_1 r_w)(I_{p1} + \sigma_3 + 2\rho_3)]\dot{\beta}\dot{\delta} + [-(I_{p1} + \epsilon_2 r_w + \rho_3)(I_{w2} + \epsilon_3 r_w + \epsilon_1 r_w) + (I_{w1} + I_{c1} + I_{p1} + \epsilon_3 r_w + \rho_1 + 2\epsilon_1 r_w)\epsilon_2 r_w]\dot{\delta}\dot{\theta}\}$
- $d_{lat} = (I_{w1} + I_{c1} + I_{p1} + \epsilon_3 r_w + \rho_1 + 2\epsilon_1 r_w)(I_{p1} + \epsilon_2 l_p) - (I_{p1} + \epsilon_2 r_w + \rho_3)^2$.

The lateral system matrix A_{lat} is perturbed by $\dot{\delta}$ and the system is disturbed by W_{lat} which is called *lateral coupling disturbance*.

The turning dynamics (Eq. (49)) can be put into the following state-space form:

$$\begin{aligned} \dot{x}_{turn} =& A_{turn}(\beta, \dot{\theta})x_{turn} + B_{turn}(\dot{\theta})\dot{\alpha} \\ &+ W_{turn}(\alpha, \beta, \gamma, \ddot{\alpha}, \ddot{\beta}, \dot{\gamma}, \ddot{\theta}), \end{aligned} \tag{70}$$

where

- $x_{turn} = \dot{\delta}$
- $A_{turn}(\beta, \dot{\theta}) = -\frac{\epsilon_1 r_w \beta \dot{\theta}}{(I_{w3}+I_{c3}+I_{p3})}$
- $B_{turn}(\dot{\theta}) = -\frac{I_{w2}\dot{\theta}}{(I_{w3}+I_{c3}+I_{p3})}$
- $W_{turn}(\alpha, \beta, \gamma, \ddot{\alpha}, \ddot{\beta}, \dot{\gamma}, \ddot{\theta}) = \frac{1}{(I_{w3}+I_{c3}+I_{p3})}[(\sigma_4 + \rho_1 + \epsilon_1 r_w)\beta\ddot{\alpha} - (I_{c2} + I_{p2} + \rho_1 + \epsilon_1 r_w)\alpha\ddot{\beta} - (\sigma_3 + \rho_3)\gamma\ddot{\beta} + (I_{p1} + \rho_3)\beta\ddot{\gamma} - (I_{w2} + \epsilon_3 r_w + \epsilon_1 r_w)\alpha\ddot{\theta} - \epsilon_2 r_w \gamma\ddot{\theta}]$.

For the turning dynamics, the system matrix A_{turn} is a function of β and $\dot{\theta}$, and the input matrix is a function of $\dot{\theta}$. The system is disturbed by W_{turn} which is called *turning coupling disturbance*.

If the perturbations in the three state-space representations are ignored, the resulting nominal state-space models can be used for designing linear controllers. The designed control laws must be able to withstand the perturbations and therefore, the understanding of these perturbations is valuable.

In linear motion, the ALP Cycle moves forward on a straight line. At steady state, the forward speed is constant and since there is no turning motion, the turning speed is zero and hence, Eqs. (69) and (70) degenerate and the perturbations in Eq. (68) disappear. Since friction is not modeled, the longitudinal lean angle β is zero.

In circular motion, the ALP Cycle moves following a circular trajectory. At steady state, the forward speed, turning speed, lean angle and pendulum angle are all constant. If the lean angle and the forward speed are sufficiently small, the turning speed is small and therefore, its squared value can be ignored. Hence, the perturbations of the longitudinal and lateral system matrices can largely be ignored. At steady state, the longitudinal and turning coupling disturbances disappear, but the lateral

https://doi.org/10.1017/S0263574715000703 Published online by Cambridge University Press

coupling disturbance becomes:

$$W_{lat}(\beta, \dot{\delta}, \dot{\theta}, \dot{\beta}, \ddot{\delta}) = \begin{bmatrix} 0 \\ 0 \\ \frac{w_{lat3nom}}{w_{lat3den}} \dot{\delta}\dot{\theta} \\ \frac{w_{lat4nom}}{w_{lat4den}} \dot{\delta}\dot{\theta} \end{bmatrix}. \tag{71}$$

where

- $w_{lat3nom} = -(I_{p1} + \epsilon_2 r_w + \rho_3)\epsilon_2 r_w + (I_{w2} + \epsilon_3 r_w + \epsilon_1 r_w)(I_{p1} + \epsilon_2 l_p)$
- $w_{lat3den} = (I_{w1} + I_{c1} + I_{p1} + \epsilon_3 r_w + \rho_1 + 2\epsilon_1 r_w)(I_{p1} + \epsilon_2 l_p) - (I_{p1} + \epsilon_2 r_w + \rho_3)^2$
- $w_{lat4nom} = -(I_{p1} + \epsilon_2 r_w + \rho_3)(I_{w2} + \epsilon_3 r_w + \epsilon_1 r_w) + (I_{w1} + I_{c1} + I_{p1} + \epsilon_3 r_w + \rho_1 + 2\epsilon_1 r_w)\epsilon_2 r_w$
- $w_{lat4den} = (I_{w1} + I_{c1} + I_{p1} + \epsilon_3 r_w + \rho_1 + 2\epsilon_1 r_w)(I_{p1} + \epsilon_2 l_p) - (I_{p1} + \epsilon_2 r_w + \rho_3)^2$.

Since the lateral coupling disturbance becomes constant at steady state, an integral action is required in lateral control to compensate this disturbance.

If a linear controller is used, the maximum lateral coupling disturbance can be estimated by using the previous results. Let us assume that the maximum angle which can be considered small is 30°. Hence, the maximum lean angle $|\alpha|_{max}$ is

$$|\alpha|_{max} = \frac{30^\circ}{K_{ls}} = \frac{0.52\ rad}{K_{ls}}.$$

With the maximum lean angle, the maximum turning speed, $|\dot{\delta}|_{max}$, is

$$|\dot{\delta}|_{max} = \frac{0.52 K_{turn}}{K_{ls}} V.$$

where V is forward speed of the robot and it is related to the wheel speed $\dot{\omega}$ by $V = r_w \dot{\omega}$. Substituting Eq. (72) into Eq. (71) and expressing the wheel speed as the forward speed, the maximum lateral coupling disturbance $max(W_{lat})$ is given by

$$max(W_{lat}) = \begin{bmatrix} 0 \\ 0 \\ \frac{|W_{lat}|_{max3num}}{|W_{lat}|_{max3den}} \frac{0.52 K_{turn}}{K_{ls} r_w} V^2 \\ \frac{|W_{lat}|_{max4num}}{|W_{lat}|_{max4den}} \frac{0.52 K_{turn}}{K_{ls} r_w} V^2 \end{bmatrix}. \tag{72}$$

where

- $|W_{lat}|_{max3num} = -(I_{p1} + \epsilon_2 r_w + \rho_3)\epsilon_2 r_w + (I_{w2} + \epsilon_3 r_w + \epsilon_1 r_w)(I_{p1} + \epsilon_2 l_p)$
- $|W_{lat}|_{max3den} = (I_{w1} + I_{c1} + I_{p1} + \epsilon_3 r_w + \rho_1 + 2\epsilon_1 r_w)(I_{p1} + \epsilon_2 l_p) - (I_{p1} + \epsilon_2 r_w + \rho_3)^2$
- $|W_{lat}|_{max4num} = -(I_{p1} + \epsilon_2 r_w + \rho_3)(I_{w2} + \epsilon_3 r_w + \epsilon_1 r_w) + (I_{w1} + I_{c1} + I_{p1} + \epsilon_3 r_w + \rho_1 + 2\epsilon_1 r_w)\epsilon_2 r_w$
- $|W_{lat}|_{max4den} = (I_{w1} + I_{c1} + I_{p1} + \epsilon_3 r_w + \rho_1 + 2\epsilon_1 r_w)(I_{p1} + \epsilon_2 l_p) - (I_{p1} + \epsilon_2 r_w + \rho_3)^2$.

Therefore, the maximum lateral coupling disturbance is related quadratically to the forward speed.

For the ALP Cycle prototype which we have constructed, using the parameters in Table I, the maximum value of lateral coupling disturbance is

$$max(W_{lat}) = \begin{bmatrix} 0 & 0 & 0.26V^2 & -0.3V^2 \end{bmatrix}^T. \tag{73}$$

4.7. Closed-loop responses

In order to illustrate the control of turning motion and the usefulness of the constants K_{lsb}, K_{ls} and K_{turn}, we perform several numerical simulations. We require some feedback control because the

https://doi.org/10.1017/S0263574715000703 Published online by Cambridge University Press

ALP Cycle is inherently unstable. In this subsection, we only use linear quadratic method with unity weighting matrices for the simulation study because we only require stability.

4.7.1. Lateral set-point control. For the ALP Cycle with the parameters given in Table I, the lateral-statics boundary K_{lsb} is 8.08° while the lateral-statics constant K_{ls} is −8.12. The value of K_{lsb} implies that the ALP Cycle can only successfully regulate its lean angle to a set point with maximum magnitude of 8.08°. The value of K_{ls} implies that if 30° is the maximum angle which can be considered to be small, then the ALP Cycle can successfully regulate its lean angle only to a set point with the maximum magnitude of

$$|\alpha_{ref}| = \frac{30^\circ}{|-8.12|} = 3.69^\circ.$$

Let us consider three cases of lateral set-point control. Cases I, II and III present the problems of controlling the lean angle, α, to the set points of 3°, 5° and 10° respectively. Linear quadratic integral (LQI) control law with the following performance index is used to stabilize the system.

$$J_{lat} = \int_0^\infty (\psi^T Q_{lat} \psi + \tau_p^T R_{lat} \tau_p)\, \mathrm{d}t. \tag{74}$$

The state vector ψ is defined as $\psi = \begin{bmatrix} \alpha & \gamma & \dot{\alpha} & \dot{\gamma} & \int_0^t \alpha \, \mathrm{d}t \end{bmatrix}^T$ and the weighting matrices are set as

$$Q_{lat} = diag(1, 1, 1, 1, 1),\ R_{lat} = 1.$$

The final control law is given by the following formula.

$$\tau_p = -K_{lat} \begin{bmatrix} \alpha - \alpha_{ref} \\ \gamma - \gamma_{ref} \\ \dot{\alpha} \\ \dot{\gamma} \\ \int_0^t (\alpha - \alpha_{ref})\, \mathrm{d}t \end{bmatrix} \tag{75}$$

$$K_{lat} = \begin{bmatrix} -230.47 & -28.67 & -51.39 & -9.33 & 1 \end{bmatrix}.$$

Numerical simulations are performed in MATLAB with the designed LQI control law and the explicit Runge–Kutta (4, 5) formula, the Dormand–Prince pair, is used to solve the ordinary differential equations involved. The simulation results are shown in Figs. 8–10 for cases I, II and III respectively.

For the three cases, α_{ref}'s are compared with K_{lsb} and $|\gamma_{ref}|$'s are computed as shown below.

- *Case I:*

$$\alpha_{ref} = 3^\circ \leq K_{lsb} = 8.08^\circ$$

$$|\gamma_{ref}| = |-8.12 \times 3^\circ| = 24.36^\circ \leq 30^\circ.$$

- *Case II:*

$$\alpha_{ref} = 5^\circ \leq K_{lsb} = 8.08^\circ$$

$$|\gamma_{ref}| = |K_{ls} \times \alpha_{ref}| = |-8.12 \times 5^\circ| = 40.6^\circ \geq 30^\circ.$$

- *Case III:*

$$\alpha_{ref} = 10^\circ \geq K_{lsb} = 8.08^\circ$$

$$|\gamma_{ref}| = |K_{ls} \times \alpha_{ref}| = |-8.12 \times 10^\circ| = 81.2^\circ \geq 30^\circ. \tag{76}$$

https://doi.org/10.1017/S0263574715000703 Published online by Cambridge University Press

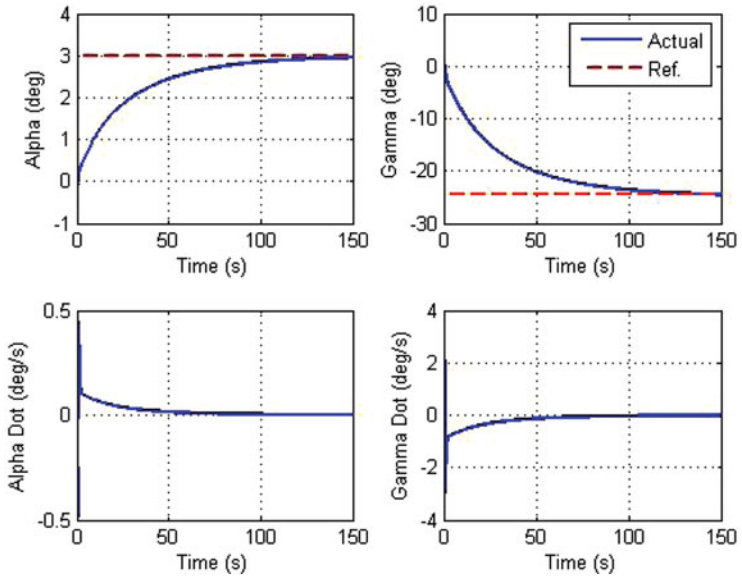


Fig. 8. The simulation results of lean-angle regulation with LQI and α_{ref} of 3°.

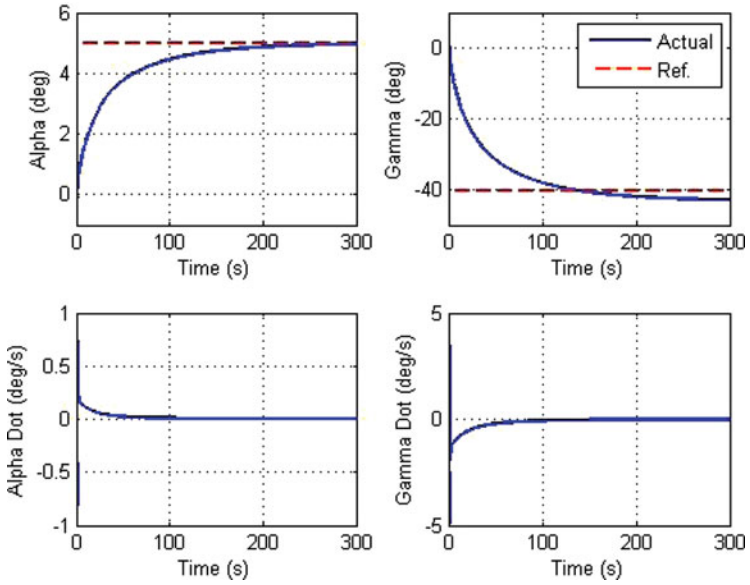


Fig. 9. The simulation results of lean-angle regulation with LQI and α_{ref} of 5°.

In Fig. 8, good set-point control is achieved. In Fig. 9, set-point control is still successful, but there is an obvious offset between γ and γ_{ref}. In Fig. 10, the system is unstable. These findings can be explained by referring to the values of α_{ref} and $|\gamma_{ref}|$ for each case. In case I, α_{ref} is less than K_{lsb}, so the set-point control is feasible. The computed γ_{ref} is less than 30° and, therefore, it can be considered small, so linear controller is expected to be successful. In case II, α_{ref} is less than K_{lsb}, so the set-point control is also still feasible. However, the computed γ_{ref} is greater than 30° and, therefore, it cannot generally be considered small, so the success of linear controller is questionable. In case III, α_{ref} is greater than K_{lsb}, so the set-point control is not feasible and, therefore, the instability of the system is completely expected and there is no need to further evaluate γ_{ref}.

In this case study, it has been shown how the lateral-statics boundary and the lateral-statics constant can be used to predict and properly set the references for lean angle and pendulum angle in the lateral set-point control.

https://doi.org/10.1017/S0263574715000703 Published online by Cambridge University Press

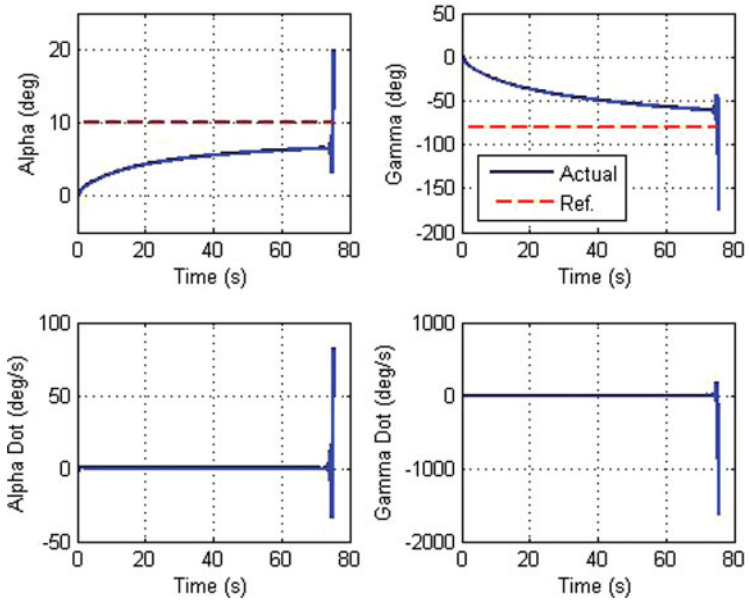


Fig. 10. The simulation results of lean-angle regulation with LQI and α_{ref} of 10°.

4.7.2. Turning-motion control. The generation and control of the turning motion are illustrated with a simple case study. This study makes use of the lateral statics-constant K_{ls} and the turning constant K_{turn} developed previously.

Let us suppose that the ALP Cycle is required to move forward with a constant speed of 1 m/s and then, at $t = 10$ s, the ALP Cycle must turn at a rate of 6°/s while maintaining its forward speed at 1 m/s. This simple scenario consists of linear and circular motions. During the linear-motion phase, the wheel-speed reference is computed as

$$\dot{\theta}_{ref} = \frac{V_{ref}}{r_w} = \frac{1 \text{ m/s}}{0.15 \text{ m}} = 6.67 \text{ rad/s} = 381.97^\circ/\text{s},$$

and, since there is no turning motion involved, the references for the lean and pendulum angles are both set to zero:

$$\alpha_{ref} = 0^\circ, \gamma_{ref} = 0^\circ.$$

In the circular-motion phase, the wheel-speed reference is not changed. Since turning motion is involved, the proper references for lean and pendulum angles need to be calculated using K_{ls} and K_{turn}.

$$\alpha_{ref} = \frac{\dot{\delta}_{ref}}{K_{turn} V_{ref}} = \frac{6^\circ/\text{s}}{-1.48 \times 1 \text{ m/s}} = -4.05^\circ$$

$$\gamma_{ref} = K_{ls} \times \alpha_{ref} = -8.12 \times (-4.05^\circ) = 32.89^\circ.$$

This scenario is simulated in MATLAB with the previously designed LQI control law as the lateral controller. A similar LQI control law for the longitudinal controller is designed with the following performance index.

$$J_{long} = \int_0^\infty (\phi^T Q_{long} \phi + \tau_w^T R_{long} \tau_w) \, \mathrm{d}t. \tag{77}$$

https://doi.org/10.1017/S0263574715000703 Published online by Cambridge University Press

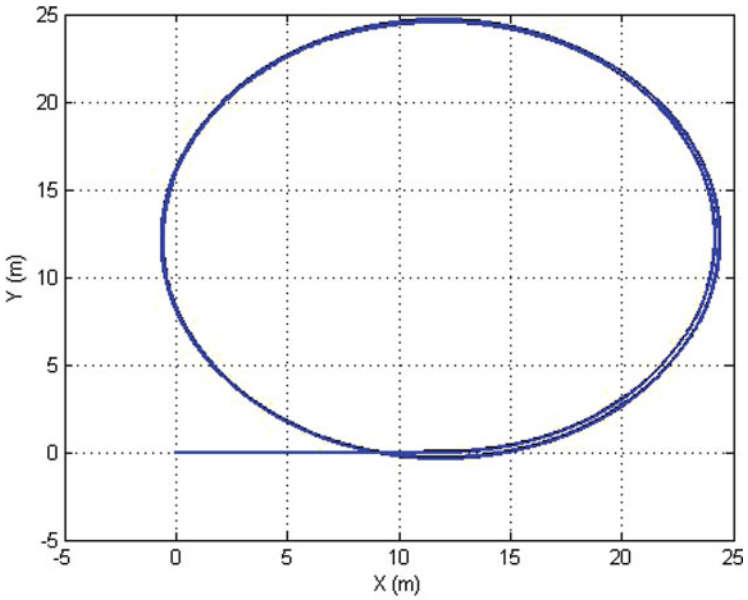


Fig. 11. The robot's trajectory on the X–Y plane.

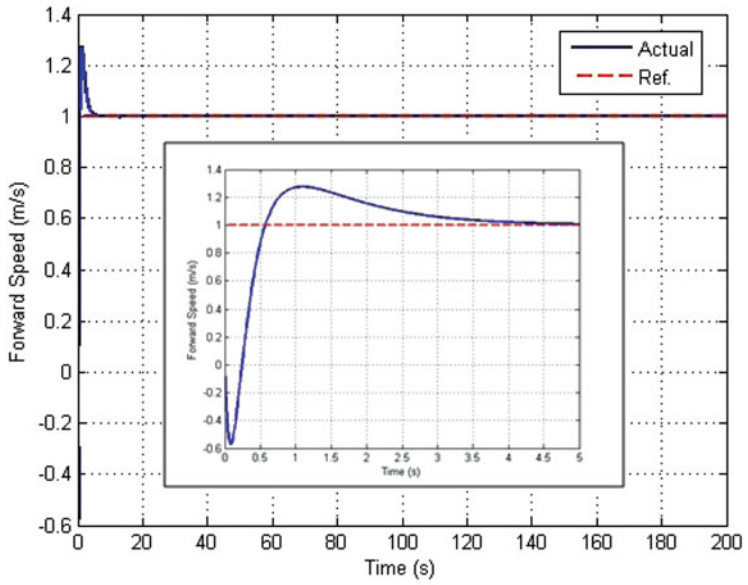


Fig. 12. The robot's forward speed (Inset shows the graph from $t = 0$ s to $t = 5$ s.).

The state vector ϕ is defined as $\phi = \begin{bmatrix} \beta & \theta & \dot{\beta} & \dot{\theta} \end{bmatrix}^T$ and the weighting matrices are set as

$$Q_{long} = diag(1, 1, 1, 1),\ R_{long} = 1.$$

The final longitudinal control law is expressed by the following formula.

$$\tau_w = -K_{long} \begin{bmatrix} \beta \\ \theta - \int_0^t (\frac{V_{ref}}{r_w})\, \mathrm{d}t \\ \dot{\beta} \\ \dot{\theta} - \frac{V_{ref}}{r_w} \end{bmatrix} \tag{78}$$

$$K_{long} = \begin{bmatrix} -35.16 & -1 & -7.74 & -1.63 \end{bmatrix}.$$

https://doi.org/10.1017/S0263574715000703 Published online by Cambridge University Press

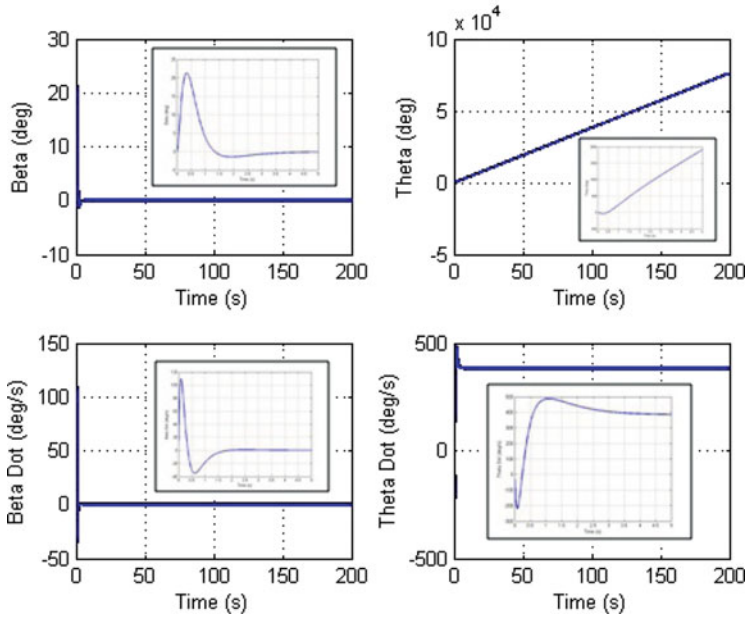


Fig. 13. The longitudinal lean angle (Beta), the wheel angle (Theta) and their rates of change (Beta Dot & Theta Dot) (inset shows the graph from $t = 0$ s to $t = 5$ s).

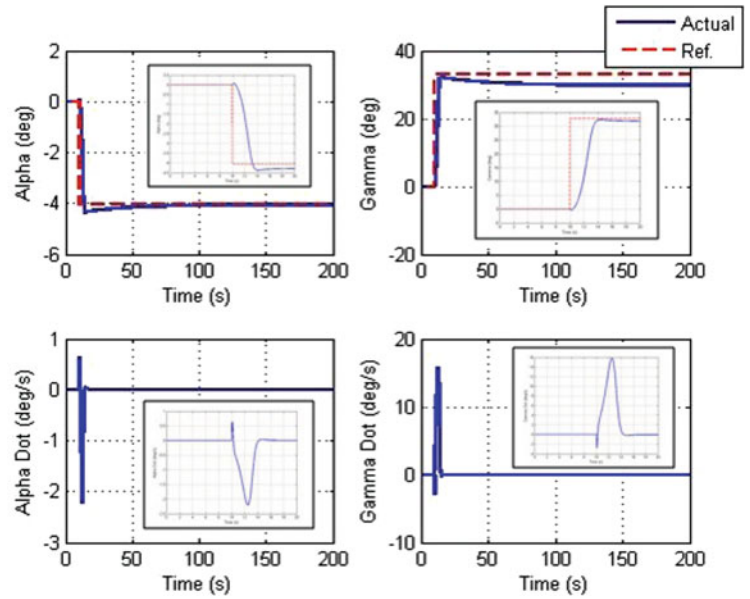


Fig. 14. The lean angle (Alpha), the pendulum angle (Gamma) and their rates of change (Alpha Dot & Gamma Dot) (inset shows the graph from $t = 0$ s to $t = 20$ s).

In this simulation case, the explicit Runge–Kutta (4, 5) formula, the Dormand–Prince pair, is used to solve the ordinary differential equations involved. The simulation results are shown in Figs. 11–19.

Figures 16 and 18 show that during the transient period, the coupling disturbances for the longitudinal and turning dynamics increase and peak up, but they quickly go down to zero as the circling motion becomes steady. Figure 17 shows that the coupling disturbance for the lateral dynamics increases, peaks up and slowly approaches constant values. These results are in agreement with the previous analysis.

https://doi.org/10.1017/S0263574715000703 Published online by Cambridge University Press

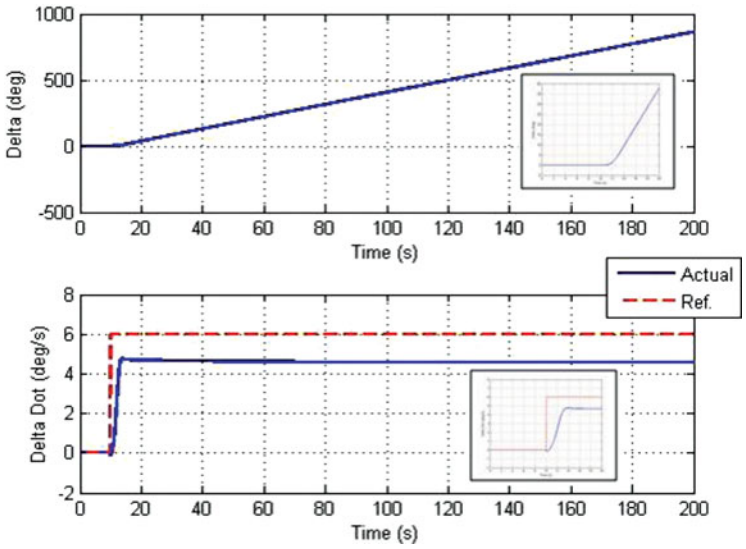


Fig. 15. The turning angle (Delta) and the turning speed (Delta Dot) (Inset shows the graph from $t = 0$ s to $t = 20$ s).

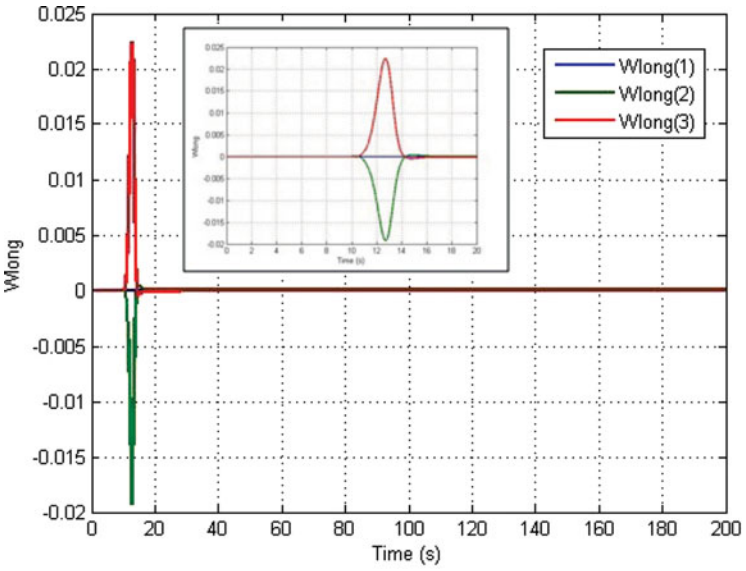


Fig. 16. The coupling disturbance for the longitudinal dynamics (W_{long}) (Inset shows the graph from $t = 0$ s to $t = 20$ s).

5. Conclusions

In this paper, the complete mathematical model of the dynamics of the lateral-pendulum unicycle robot has been derived and analyzed. From the dynamic model, three constants are derived namely (1) the lateral-statics boundary, which dictates the feasibility of the lateral set-point control, (2) the lateral-statics constant, which is required in the lateral set-point control to calculate the proper pendulum-angle reference, given a desired lean-angle reference and (3) the turning constant, which is necessary to compute the approximate lean-angle reference required to achieve a certain turning speed in the turning-motion control. In addition, with the turning constant, the minimum path curvature which the robot can successfully follow without losing its stability has been evaluated. The behaviors of the longitudinal, lateral and turning dynamic couplings have been investigated and it has been shown how integral action is needed in the lateral controller, while it is not required in the longitudinal and turning controllers. Due to their dependence on the robot parameters, the lateral-statics boundary, lateral-statics constant and turning constant can be used to design a high-performance prototype

https://doi.org/10.1017/S0263574715000703 Published online by Cambridge University Press

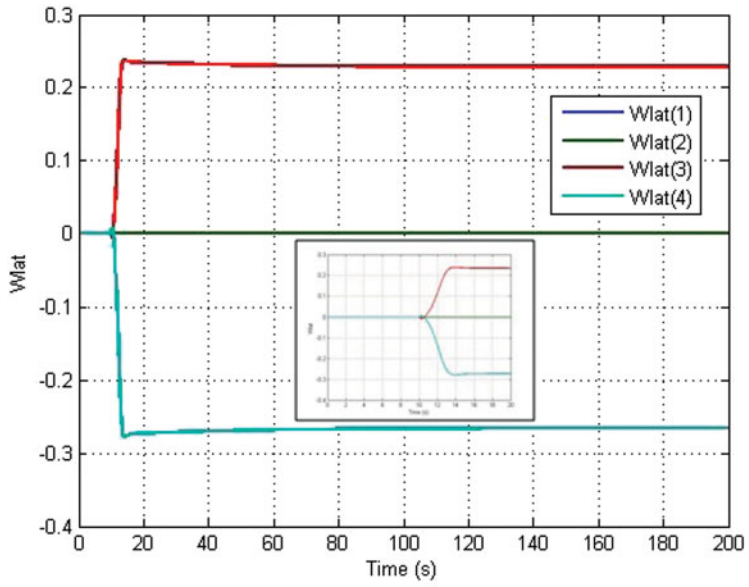


Fig. 17. The coupling disturbance for the lateral dynamics (W_{lat}) (Inset shows the graph from $t = 0$ s to $t = 20$ s).

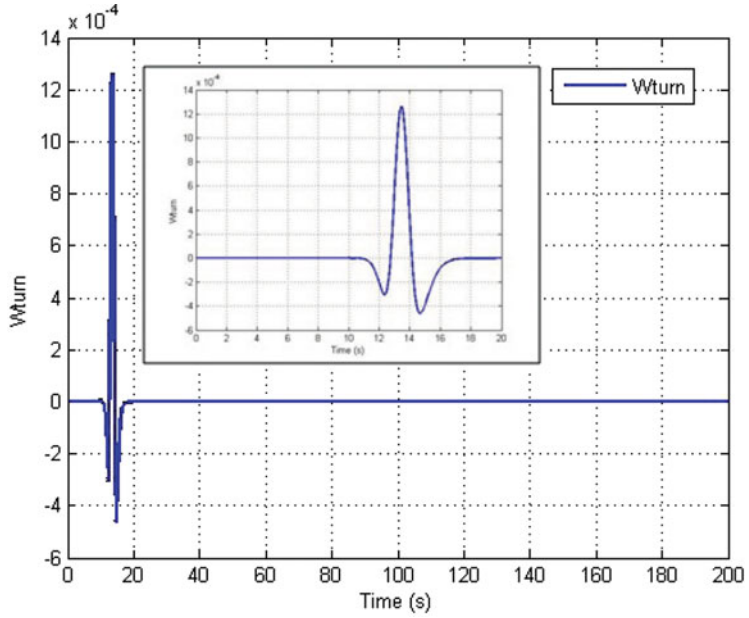


Fig. 18. The coupling disturbance for the turning dynamics (W_{turn}) (Inset shows the graph from $t = 0$ s to $t = 20$ s).

capable of leaning sideways at larger angle and following sharper path. The results presented in this paper will enable thorough simulation study and systematic control design for this particular type of robot.

As the focus of this paper is on the modeling and analysis of the robot dynamics, the standard linear quadratic method is used to design the controllers in order to illustrate how the derived formulae can be used in control design. In the future, in addition to the experimental work to be done with the developed prototype, we plan to investigate the feasibility of using fuzzy controller to design both the longitudinal controller and the lateral controller. As fuzzy controller is nonlinear by nature, it may be a more suitable solution to deal with the nonlinearity of this robot dynamics, compared to the linear quadratic control.

https://doi.org/10.1017/S0263574715000703 Published online by Cambridge University Press

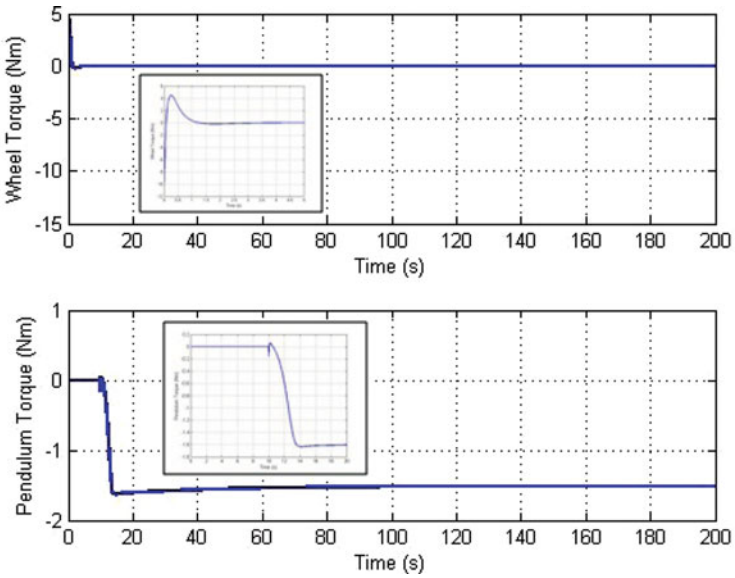


Fig. 19. The wheel torque and the pendulum torque (Inset shows the graph from $t = 0$ s to $t = 20$ s).

References

1. A. Schoonwinkel, Design and Test of a Computer Stabilized Unicycle *Ph.D. Thesis* (Stanford University, 1987).
2. D. W. Vos and A. H. von Flotow, "Dynamics and Nonlinear Adaptive Control of an Autonomous Unicycle: Theory and Experiments," *Proceedings of 29th Conference on Decision and Control*, Honolulu, Hawaii, USA (1990).
3. H. Jin, J. Hwang and J. Lee, "A balancing control strategy for a one-wheel pendulum robot based on dynamic model decomposition: Simulations and experiments," *IEEE/ASME Trans. Mech.* **16**(4), 763–768 (Aug. 2011).
4. J.-X. Xu, A. Al Mamun, Y. Daud, "Pendulum-Balanced Autonomous Unicycle: Conceptual Design and Dynamics Model," *Proceedings of the 5th IEEE International Conference on Robotics, Automation and Mechatronics*, Qingdao, China (2009).
5. M. W. Spong, "Swing-up control of the Acrobot," *IEEE International Conference on Robotics and Automation* (1994).
6. M. W. Spong, S. Hutchinson and M. Vidyasagar, *Robot Modeling and Control* (Wiley, New Jersey, USA, 2005).
7. R. Nakajima, T. Tsubouchi, S. Yuta and E. Koyanagi, "A Development of a New Mechanism of an Autonomous Unicycle," *Proceedings of IROS* (1997).
8. S. Brent Cardini, "A history of the monocycle: Stability and control from inside the wheel," *Control Syst. Mag.* **26**(5), 22–26 (Oct. 2006).
9. S. Majima, T. Kasai and T. Kadohara, "A design of a control method for changing yaw direction of an underactuated unicycle robot," *Proceedings of TENCON* (2006).
10. S. Y. Seo, S. Hee Kim, S.-H.Lee, S. H. Han and H. Sung Kim, "Simulation of Attitude Control of a Wheeled Inverted Pendulum," *International Conference on Control, Automation and Systems* (2007).
11. Y. Fujimoto and S. Uchida, "Three dimensional posture control of mono-wheel robot with roll rotatable torso," *Proceedings of International Conference on Mechatronics*, Kumamoto, Japan (2007).
12. Z. Sheng and K. Yamafuji, "Postural stability of a human riding a unicycle and its emulation by a robot," *IEEE Trans. Robot. Autom.* **13**(5), 709–720 (Oct. 1997).

https://doi.org/10.1017/S0263574715000703 Published online by Cambridge University Press